"Predictive Optimal Control of Active and Passive Building Thermal Storage Inventory"

Topical Report

Reporting Period Start Date: January 1, 2003

Reporting Period End Date: December 17, 2003

Principal Authors:

Principal Investigator:

Gregor P. Henze, Ph.D., P.E.
Assistant Professor of Architectural Engineering
University of Nebraska – Lincoln
College of Engineering and Technology
Omaha, Nebraska 68182-0681

Co-Principal Investigator:

Moncef Krarti, Ph.D., P.E.
Associate Professor of Architectural Engineering
University of Colorado at Boulder
College of Engineering
Boulder, Colorado 80309-0428

Date Report was Issued: December 2003

DOE Award Number:

DE-FC-26-01NT41255

Name and Address of Submitting Organization:

Primary Organization:

University of Nebraska – Lincoln
303 Canfield Administration Building
Lincoln, Nebraska 68588-0430

Subcontractor:

The Regents of the University of Colorado
University of Colorado at Boulder
Boulder, Colorado 80309-0428

Disclaimer

Abstract

Cooling of commercial buildings contributes significantly to the peak demand placed on an electrical utility grid. Time-of-use electricity rates encourage shifting of electrical loads to off-peak periods at night and weekends. Buildings can respond to these pricing signals by shifting cooling-related thermal loads either by precooling the building's massive structure or the use of active thermal energy storage systems such as ice storage. While these two thermal batteries have been engaged separately in the past, this project investigates the merits of harnessing both storage media concurrently in the context of predictive optimal control.

This topical report describes the demonstration of the model-based predictive optimal control for active and passive building thermal storage inventory in a test facility in real-time using time-of-use differentiated electricity prices without demand charges. The laboratory testing findings presented in this topical report cover the second of three project phases. The novel supervisory controller successfully executed a three-step procedure consisting of 1) short-term weather prediction, 2) optimization of control strategy over the next planning horizon using a calibrated building model, and 3) post-processing of the optimal strategy to yield a control command for the current time step that can be executed in the test facility.

The primary and secondary building mechanical systems were effectively orchestrated by the model-based predictive optimal controller in real-time while observing comfort and operational constraints. The findings reveal that when the optimal controller is given imperfect weather forecasts and when the building model used for planning control strategies does not match the actual building perfectly, measured utility costs savings relative to conventional building operation can be substantial. This requires that the facility under control lends itself to passive storage utilization and the building model includes a realistic plant model.

The savings associated with passive building thermal storage inventory proved to be small because the test facility is not an ideal candidate for the investigated control technology. Moreover, the facility's central plant revealed the idiosyncratic behavior that the chiller operation in the ice-making mode was more energy efficient than in the chilled-water mode. Field experimentation (Phase III) is now required in a suitable commercial building with sufficient thermal mass, an active TES system, and a climate conducive to passive storage utilization over a longer testing period to support the laboratory findings presented in this topical report.

Table of Contents

1 Introduction

1.1 Background

The energy consumption of commercial buildings contributes a substantial 18% or 17.4 out of 97.4 quadrillion Btu ("quads") to the total U.S. primary energy consumption (EIA/DOE, 2002). Aggravated by a surge in the use of office equipment combined with the associated demand for cooling energy, electricity is responsible for 75% of the primary energy consumption in commercial buildings, about 800 million metric tons of carbon emissions per year, and over $65 billion of utility cost. Harnessing the efficiency potential in current and future buildings will be instrumental in attenuating the growth of energy consumption and electrical demand as well as the nation's dependency on an uninterrupted supply of fossil fuels. This constitutes the motivation for this work.

The equipment and systems providing thermal comfort and indoor air quality consume 42% of the total energy used in buildings (A.D. Little, 1999). Energy use and utility cost can be reduced by increasing the efficiency of building systems, by distributing thermal energy more efficiently and by more closely meeting the needs of building occupants. The energy efficiency of system components for heating, ventilating, and air-conditioning (HVAC) has improved considerably over the past 20 years (ARI, 1999; American Standard, 1999).

In contrast to energy conversion equipment, less improvement has been achieved in thermal energy distribution, storage and control systems in terms of energy efficiency and peak load reduction potential. Advancements are also needed to improve thermal storage systems, control systems and systems integration from a whole building perspective while meeting occupant comfort and performance requirements (NETL/DOE, 2003). This topical report implements and evaluates a novel supervisory real-time control strategy in a test facility in order to tackle several of these needed advancements.

Our approach employs the simultaneous utilization of *active* and *passive* building thermal storage inventory under model-based predictive optimal supervisory control. In the definition of this article, 'active' denotes that thermal storage systems, such as chilled-water or ice storage, require an additional fluid loop to charge and discharge the storage tank and to deliver cooling to the existing chilled water loop. Using building thermal capacitance through nighttime precooling is 'passive', since it requires no additional heat exchange fluid other than the conditioned air stream. The objective function for the model-based predictive controller discussed in this topical report is the minimization of building operating costs while observing constraints on occupant thermal comfort, indoor environmental quality, and HVAC equipment operation.

1.2 Review of Past Work

Cooling of commercial buildings contributes significantly to the peak demand placed on an electrical utility grid. Time-of-use electricity rates encourage shifting of electrical loads to off-peak periods at night and weekends. Buildings can respond to these pricing signals by shifting cooling-related electrical loads either by precooling the building's massive structure, by the use of an active energy storage system only, or by a combination of both thermal reservoirs. Henze et al. (1997) developed a predictive optimal controller for active thermal energy storage (TES) systems and investigated the potential benefits of optimal control for ice storage systems under real-time pricing in order to minimize the cost of operating a central cooling plant. It was found that in the presence of complex rate structures, i.e., real-time pricing rates that change on an hourly basis, the proposed optimal controller has a significant performance advantage over conventional control strategies while requiring only simple predictors.

Braun (2003) surveyed research on passive building thermal storage utilization, i.e., the precooling of a building's thermal mass during nighttime in order to shift and reduce peak cooling loads in commercial buildings. He identified considerable saving potential for operational costs, even through the total zone loads may increase. Opportunities for reducing operating expenses are due to four effects: reduction in demand costs, use of low cost off-peak electrical energy, reduced mechanical cooling resulting from the use of cool nighttime air for ventilation precooling, and improved mechanical cooling efficiency due to increased operation at more favorable part-load and ambient conditions. However, these benefits must be balanced with the increase in the total cooling requirement that occurs with the precooling of the thermal mass. Therefore, the savings associated with load shifting and demand reduction are very sensitive to utility rates, building and plant characteristics, weather conditions, occupancy schedules, operation condition, the method of control, and the specific application. In general, better opportunities for effective precooling exist for higher ratios of on-peak to off-peak rates, longer on-peak periods, heavy-mass building construction with a small ratio of the external area to the thermal mass, and for cooling plants that have a good part-load characteristics for which the best performance occurs at about 30% of the design load.

The *combined* usage of both active and passive building thermal storage inventory under optimal control has recently been investigated by Henze et al.(2004a) for the reduction of electrical utility cost in the context of common time-of-use rate differentials. The objective function used in the optimization is the total utility bill including the cost of heating and a time-of-use electricity rate without demand charges. The analysis showed that when an optimal controller for combined utilization is given perfect weather forecasts and when the building model used in the model-based predictive control perfectly matches the actual building, the utility cost savings are significantly greater than either storage, but less than the sum of the individual savings and the cooling-on-peak electrical demand can be drastically reduced.

While Henze et al.(2004a) established the theoretical maximum performance of this novel control strategy, further research by Henze et al.(2004b) explored how strongly prediction uncertainty in the required short-term weather forecasts affects the controller's cost saving performance. The best prediction accuracy was found for a bin model that develops a characteristic daily profile from observations collected over the past 30 or 60 days. Assuming that the building thermal response is perfectly represented by the building model, i.e., there is no mismatch between the modeled and actual building behavior, the predictive optimal control of active and passive building thermal storage inventory involving weather predictions lead to utility cost savings that are only marginally inferior compared to a hypothetical perfect predictor that exactly anticipates the weather during the next planning horizon. The primary finding is that it takes only very simple short-term prediction models to realize almost all of the theoretical potential of this storage control technology.

Liu and Henze (2004) investigated the impact of five categories of building modeling mismatch on the performance of model-based predictive optimal control of combined thermal storage using perfect prediction. It was found that for an internal heat gain dominated commercial building, the deviation of building geometry and zoning from the reference building only marginally affects the optimal control strategy; reasonable simplifications are acceptable without loss of cost saving potential. In fact, zoning simplification may be an efficient way to improve the optimizer performance and save computation time. The mass of the internal structure did not strongly affect the optimal results; however, it did change the building cooling load profile, which in turn will affect the operation of the active storage (TES) system. Exterior building construction characteristics were found to impact building passive thermal storage capacity. Thus, it is recommended to make sure the construction material is well modeled. Furthermore, zone temperature setpoint profiles and TES performance are strongly affected by mismatches in internal heat gains, thus efforts should be made to keep the internal gain mismatch as small as possible. Efficiency of the

building energy system has no direct impact on the building cooling load, but it affects both, zone temperature setpoints and active TES operation because of the coupling to the cooling equipment. Mismatch in this category may be significant.

On the background of these findings, a predictive optimal controller for the combined usage of active and passive thermal storage that accounts for uncertainty in predictive variables and model mismatch was developed and verified in the context of the presented work. Once the supervisory controller was implemented in the laboratory setting, the test facility was controlled by the optimizer in real-time, which to the authors' knowledge has not been done before. This topical report describes the implementation of the real-time control strategy and evaluates its benefits with respect to HVAC energy consumption and cost reduction. In addition, model accuracy and constraint compliance will be examined. The report concludes with a recreation of the experiment in a simulation environment during which previously experienced problems such as the interruption of the communication to the building automation system were avoided.

2 Description of Test Facility

2.1 General Background on ERS

The building used in this study to investigate the potential of the optimal controller is the Energy Resource Station (ERS); operated by the Iowa Energy Center (IEC). The ERS is a unique demonstration and test facility wherein laboratory-testing capabilities are combined with real building characteristics. The ERS is capable of simultaneously testing two full-scale commercial building systems side-by-side with identical thermal loading. Located on the campus of the Des Moines Area Community College (DMACC) in Ankeny, Iowa; it has a latitude of 41.7° North, a longitude of 93.6° West, and an elevation of 286 m above sea level. The facility is orientated for a true north/south solar alignment and no surrounding objects and no trees block solar radiation on the ERS, except for the north side of the building that has a fenced in mechanical yard with a concrete floor.

The ERS building, a single story structure with a concrete slab-on-grade, has a height of 4.6 m and a total floor area of 855 m^2, divided into a general area (office space, service rooms, media center, two classrooms, etc.), and two sets of identical test rooms, labeled '*A*' and '*B*'; adjacent to the general area. The eight test rooms are organized in pairs with three sets of zones having one exterior wall (east, south, and west) and one set that is internal. Figure 1 presents a layout or the ERS including the four sets of identical test rooms used for the experiment.

The opaque exterior envelope of the ERS is composed of several layers of construction materials with a thermal mass outside of the insulation. The percentage of the window area to exterior wall area is 15% on the east side, 16% on the west side, 32% on the south, and no windows on the north (Price and Smith, 2000).

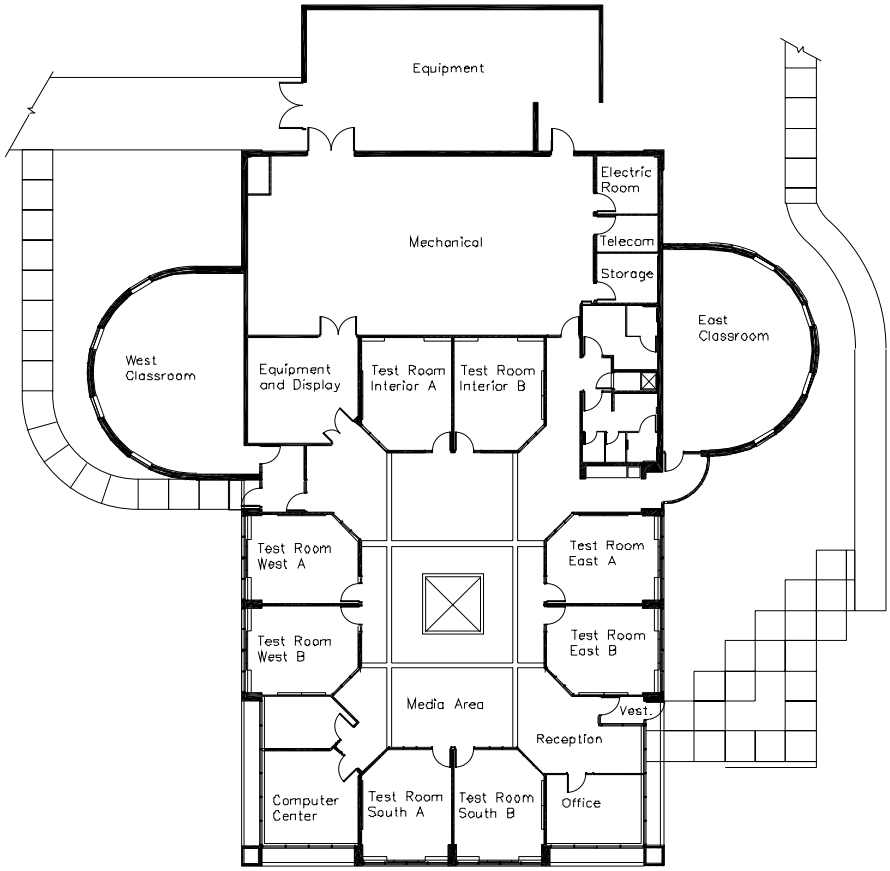

Figure 1: Layout of the test facility, the Energy Resource Station (ERS), Ankeny Iowa.

2.2 Primary and Secondary HVAC Systems

The ERS is equipped with a central heating plant consisting of a natural gas-fired boiler and a cooling plant comprising three nominal 35 kW air-cooled chillers for both chilled-water and ice-making modes. The chilled-water loop is filled with 22% propylene glycol water solution. In addition, the building includes a 440 kWh internal melt ice-on-tube thermal energy storage tank as well as pumps and auxiliary equipment needed to provide cooling. District cooling can be provided by the DMACC campus chilled water plant but was not used in this experiment. Hence, several modes of operation between these sources of cooling are possible in order to supply chilled water to the air handling units (AHU). The chilled water loop is a primary-secondary flow arrangement with dedicated constant-volume chiller pumps and secondary variable-flow distribution pumps in the AHU loop under VFD control.

The secondary HVAC system consists of three AHUs that condition the building: Test rooms A and B are served by two similar single-duct VAV with reheat AHU systems A and B, and the general area is served by a similar but larger AHU-1. An overhead air distribution system utilizing pressure-independent VAV boxes supplies air to each test room using hydronic or 3-stage electrical resistance reheat.

Finally, there is an on-site weather station with measurements of outdoor air dry-bulb temperature, relative humidity, wind speed and direction, atmospheric pressure, total normal incidence solar flux, and global horizontal solar flux.

2.3 Investigated Test Rooms

The experiment was executed in the test rooms A and B, each with a net floor area of 24.8 m^2 and carpeted floor. The ceiling height is 2.6 m and there is a plenum above the suspended ceiling with a height of 1.7 m. Having the same geometry and construction specifications, but being thermally isolated from each other; the identical pairs A and B experience the same heating and cooling load. The window area of the exterior zones consists of double-pane 6.4 mm clear insulating glass and measures 6.9 m^2. During the test, these windows were covered with fully open external blinds. Furthermore, to reduce thermal coupling to the general area, the interior windows between the test rooms and the general area were covered with 12.7 mm dry wall paper. Following the suggestion of Braun et al. (2002) at the ERS, additional mass was added to the interior test rooms A and B in the form of two rows of standard concrete cinder block, 3.05 m long and each stacked three layers high. The walls were located near the middle of each interior room.

The rooms are unoccupied; however, false internal heat gains can be introduced using baseboard heaters and lights to simulate the occupancy schedule of a typical building. Test rooms A are equipped with 2-stage lighting whereas test rooms B are fitted with dimming electronic ballasts, both with a maximum wattage of 585 W. The baseboard heater at each zone can operate at two stages with a maximum output of 1.8 kW (900 W per stage).

A comfort sensor measuring the air temperature, humidity, and wind speed was placed in the middle of the rooms. Conditioned air at a temperature of 13°C was supplied to the test rooms by two ceiling mounted diffusers in order to maintain the room temperature within a range of 20°C and 24°C during time of occupancy. The interior flow rate throughout the occupied period was characterized by a minimum flow of 94 L/s and a maximum flow of 189 L/s. Finally, all test rooms were kept looked throughout the period of the experiment in order to avoid disturbance and interruptions. These conditions were applied to all eight test rooms.

The ERS is not a particular good candidate for the use of building thermal mass as documented by Braun (2003) due to two reasons: (i) it is a light-weight single-story structure with a high exterior surface area to volume ratio and (ii) significant thermal coupling with the ground, the ambient and the zones adjacent to the test rooms is present. Furthermore, the test zones are not equipped with a representative amount of furniture and the floor is carpeted, which reduces thermal coupling to the massive structure.

2.4 Assumptions for Predictive Optimal Control

The simulated occupied period extends from 8 a.m. to 5 p.m. each day including weekends. During this time, baseboard heaters are applied at one stage (0.9 W) and they are turned off during the remaining hours. Furthermore, one stage of lighting (360 W) is employed from 7 a.m. to 6 p.m. The applied utility rate structure assumes an on-peak electricity rate of $0.20/kWh from 9 a.m. to 7 p.m. and an off-peak electricity rate of $0.05/kWh the remaining hours. Demand charges are not levied.

Of the available equipment, the HVAC system during the test consists of two chillers, namely a main and a dedicated precooling chiller, and the ice-based TES system. The main chiller that is responsible for charging the TES tank and meeting on-peak cooling loads operates in the chilled-water mode with a coefficient-of-performance (COP) of 2.1 and in the ice-making mode (charging the TES) with a COP of 2.4. The COPs were validated through repeated tests at the ERS. Consequently, meeting cooling loads through the usage of ice storage is more attractive from an energy consumption perspective than standard chilled-water operation.

Initial tests investigating conventional control strategies revealed that charging of the TES system takes noticeably more time than estimated by the controller, which was traced back to a significantly reduced chiller capacity to only 50% in the ice-making mode. Further, it was deter-

mined that the ice storage system behaves very nonlinearly below 20% and above 90% state-of-charge (SOC). Since the model employed in the predictive optimal control assumes a linear change in SOC with the charging and discharging rates, the SOC was limited to an available range of 25% to 75%, effectively cutting the storage capacity in half to 220 kWh.

The dedicated precooling chiller with a measured COP of 3.4 is assigned to flush the building with cool air during nighttime and, consequently, to precool the building's massive structure and furniture. Both chillers cannot simultaneously supply chilled water to the AHU.

The outdoor air ventilation is governed by a return air temperature economizer that allows for free cooling when the ambient air conditions are favorable. The minimum outdoor intake damper is restricted to a position of 45% open for AHU A and 37.5% open for AHU B to ensure 20% of ventilation air at design air flow conditions.

Simulations and experiments in the same facility conducted by Braun et al. (2002) revealed that there exists significant thermal coupling between the test rooms and the adjacent general area. As a result, there would be significant energy transfer between zones when utilizing different zone temperature strategies. Therefore, the decision was made to control the entire facility with a uniform schedule for occupancy and a similar control strategy. As a result, the evaluation of optimal and conventional control strategies is accomplished by comparing measured results under optimal control and simulated results using conventional control and not by comparing measured results from test rooms A under optimal and test rooms B under conventional control.

The general area was conditioned with 13°C supply air from 7 a.m. to 5 p.m. with a zone temperature setpoint of 22°C. During unoccupied periods, temperatures were allowed to flow. Outside air intake was controlled by an economizer, restricting the minimum damper position to 10%.

It was verified by ERS personnel that all sensors were sufficiently calibrated and over 750 monitoring points at minute-by-minute intervals were recorded during the experiments.

3 Description of Implemented Predictive Control Strategy

3.1 Overview

In this study we employed a sequential approach to model-based control: 1) short-term forecasting, 2) optimization, and 3) post-processing and control command implementation as shown in Figure 2. A real-time weather station provides the current weather data to the short-term weather predictor. This predictor provides an improved forecast for the next planning horizon to the optimal controller, which adjusts the control variables in the model according to Figure 3 until convergence is reached. The optimal solution is passed to a post-processor that interprets the optimal results and turns them into commands understood by the building automation system of the facility under control. The building is modeled in TRNSYS (2003), while the general purpose technical computing environment Matlab (2000) including the optimization toolbox was used to interface with the building simulation program.

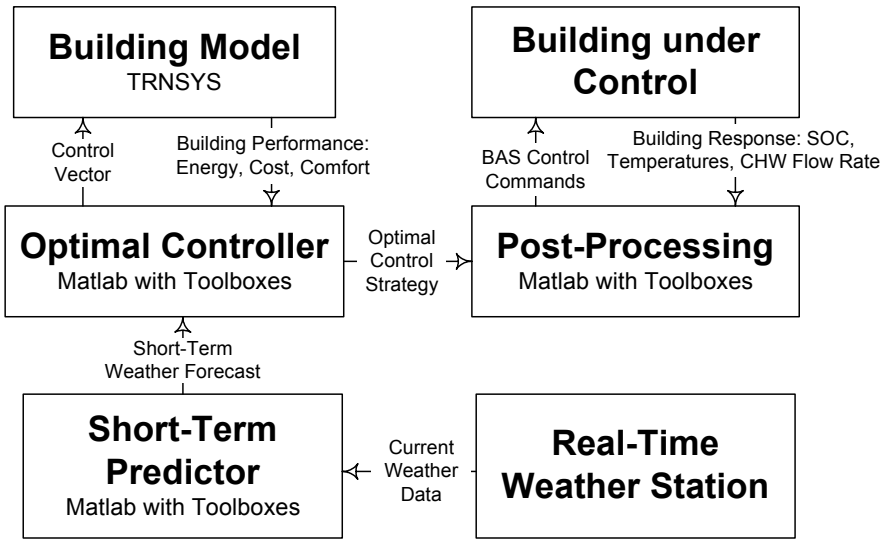

Figure 2: Real-time predictive optimal control schematic.

3.2 Prediction

A 30-day bin predictor model was found to provide the most accurate weather forecasts for a range of models tested in previous research by Henze et al. (2004b). The predicted variables include ambient air dry-bulb temperature, relative humidity, global solar radiation, and direct normal solar radiation. The assumption underlying the prediction procedure is that the actual time series will exhibit a behavior similar to a reference pattern, developed by rendering bin estimates. For a planning horizon of L = 24 hours, the bin model develops the characteristic profile on the basis of observations collected over the past 30 days. The forecast is made by shifting the L-hour profile such that the predicted value for the current hour k^* coincides with the actual measured value by the weather station at the ERS. Hence, the forecast bin values are computed from

$$\left\{\hat{X}_t\right\} = \frac{1}{d}\sum_{n=1}^{d} X_{t-24n}, \quad t \in [k^*, k^* + L], \tag{1}$$

where d is the number of past days used to compute the bins, and X_t is the observed variable. The 24-hour forecast is handed over to the optimal controller that uses these values among others to estimate the building cooling load profile for the next L hours.

3.3 Real-Time Model-Based Predictive Optimal Control

The optimal controller governing the two sources of thermal energy storage can minimize an objective function of choice including total energy consumption, energy cost, occupant discomfort, or a combination of these. In this study, the real-time controller was charged to minimize operating cost for time-of-use differentiated electricity and fixed-cost natural gas by adjusting global zone temperature setpoints $T_{Z,SP}$ for the passive storage and a dimensionless charge/discharge rate u for the active storage.

Optimal control is defined as that control trajectory that minimizes the total monthly utility bill C_m for electricity and heating:

$$\begin{aligned} J_m &= \min C_m = \min\left\{C_{elec,m} + C_{heat,m}\right\}, \text{ where} \\ C_{elec,m} &= \sum_{k=1}^{K_m} r_{e,k} P_k \Delta t_h; \quad C_{heat,m} = \sum_{k=1}^{K_m} r_h \dot{Q}_{heat,k} \Delta t_h \end{aligned} \tag{2}$$

where $r_{e,k}$ is the energy rate for electricity according to the utility tariff in effect for time k, K_m is the number of hours in the current month, Δt_h is a time increment of one hour, r_h is the unit cost of heat delivered, and $\dot{Q}_{heat,k}$ is the heating demand from zone reheat in hour k.

To apply fixed-horizon optimal control to an infinite-horizon problem such as the given real-time control (it could go on indefinitely), closed-loop optimization (CLO) is employed, i.e., the predictive optimal controller carries out an optimization over a predefined planning horizon L and of the generated optimal strategy only the first action is executed. At the next time step the process is repeated. The final control strategy of this near-optimal controller over a total horizon of K steps is thus composed of K initial control actions of K optimal strategies of horizon L, where $L < K$. By moving the time window of L time steps forward and updating the control strategy after each time step, a new forecast is introduced at each time step and yields a control strategy, which is different from the strategy found without taking new forecasts into account. Since we optimize over a planning horizon of L hours, we can only minimize an approximate cost function C_L, which allows for the determination of a near-optimal strategy, whose cumulative utility cost approaches the desired J_m at the end of the billing period.

Figure 3 illustrates how the minimal utility cost J_L over time horizon L is determined. At time zero and starting with initial zone temperature setpoints $\{T_{Z,SP}\}_{init}$ halfway between the upper and lower bounds and no active storage utilization $\{u\}_{init} = 0$, the passive storage inventory is optimized to minimize C_L. As a result, the optimal building cooling load profile is computed and handed over to the active storage optimization, which calculates an optimal TES charge/discharge strategy. In a second pass, the optimal active storage utilization strategy and the previously found optimal zone temperature setpoint profile are employed to determine the new optimal zone temperature setpoint profile and optimal utility cost J_L. This cycle is repeated until the optimal cost J_L converges. Typically, convergence is attained after 2 to 3 iterations. Previously optimal solutions are stored as starting values for subsequent optimizations to reduce execution time. We refer to Henze et al. (2004a) for a detailed description of the model-based predictive optimal controller for building thermal storage inventory.

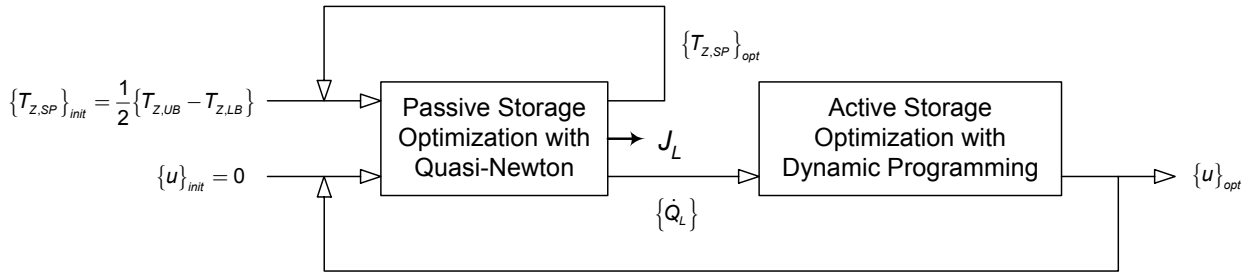

Figure 3: Iterative sequential optimization of utility cost C_L

At each time step *k*,* the model-based controller derives the following four operational parameters for the active TES system from the optimal charge/discharge rate u_{k^*}: charging load for the main chiller (Q_{charge}), discharging load for the active TES system ($Q_{discharge}$), remaining cooling load for the main chiller (Q_{main}), and cooling load met by the precooling chiller ($Q_{precool}$). Rules incorporated in the building model ensure that a) charging and discharging cannot occur simultaneously; b) when the main chiller charges the active TES tank, any building cooling load has to be met by the precooling chiller; and c) when the TES system is discharged, any remaining building cooling load has to be met by the main chiller.

3.4 Post-Processing

A post-processing computer program was developed for the ERS test facility to translate the optimal results produced by the model-based controller into commands, which can be understood by the building automation system and executed by the ERS HVAC system. The post-processing program sketched in Figure 4 sequentially executes the following operations every hour: (a) setup of a communication channel between the optimal controller environment and the BAS using a proprietary general-purpose communication software, (b) reading the optimal results from the optimal control and the required values from the BAS, (c) conversion of optimal results into control commands, and (d) sending the new control commands to the BAS.

The following post-processing procedure is executed: First, the room air temperature setpoint is sent directly to the BAS. Next, the cooling discharge rate of the TES is accomplished by sending the TES leaving water temperature as a setpoint for the TES mixing valve local loop control. The leaving water temperature $T_{LW,TES}$ is calculated from $\dot{Q}_{\text{discharge}} = \dot{m} c_p \left(T_{EW,TES} - T_{LW,TES} \right)$, where flow rate ($\dot{m}$) and entering water temperature ($T_{EW,TES}$) are read from the BAS.

During occupancy, the cooling output of the main chiller, operating with a constant cooling output in one of two stages, is accomplished by pulse width modulation (PWM). The PWM algorithm translates the optimal control result Q_{main} into a chiller stage and minutes of operating time during the next hour. The PWM time period was 20 min. Thus, the total chiller operating time is distributed over three PWM periods per hour. Operational constraints have also been taken into account. For example, there are at least five minutes between two periods of chiller operation in order to avoid the chiller cycling too frequently. Moreover, if the calculated main chiller load results in an operating time less than 5 minutes, than the chiller will operate 5 min. The precooling chiller is operated by the existing on-off control algorithm without PWM to maintain the global zone temperature setpoint $T_{Z,SP}$ in the building.

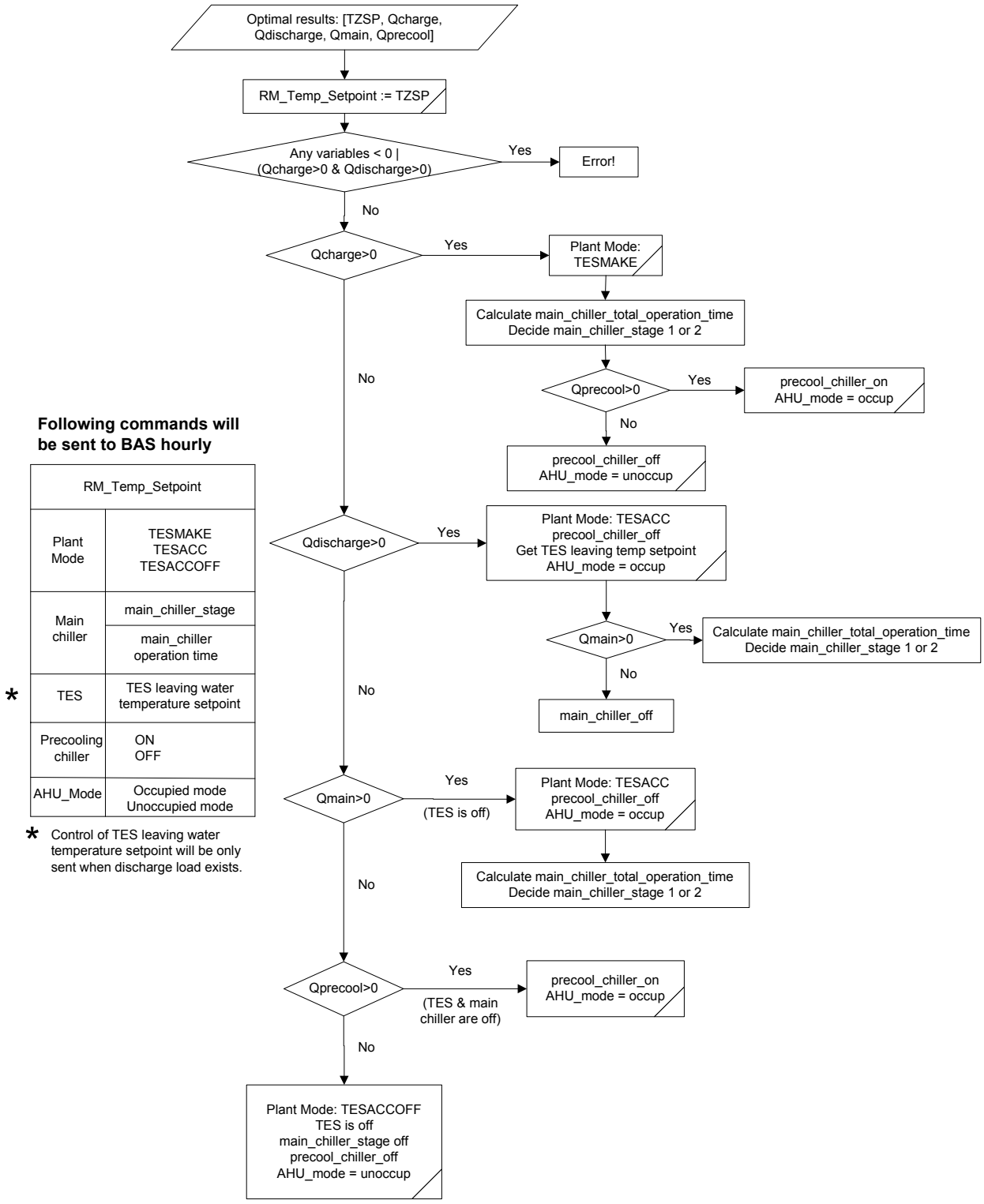

Figure 4: Post-processing program flow chart.

3.5 Control Command Execution

The building automation system requires five plant modes, which had previously been defined for the ERS test facility and had been modified to accommodate the predictive optimal control. A plant mode has to be selected before a command from the post-processing program can be sent to the HVAC system. The three of the available plant modes used in the context of our experiment were: TESMAKE plant mode which represents charging of the active TES system, TESACC plant mode in which the test rooms are conditioned by the main chiller and/or the active TES system, and TESACCOFF where the entire HVAC system is turned off. In addition, the BAS enables the air-handling unit fans based on the existence of a cooling load on the AHU cooling coils. In summary, the post-processing program obtains the optimal results from the controller, converts the values into comprehensible commands, selects a plant mode and forwards the commands using the communication channel to the BAS.

4 Description of Conventional Control Strategies

Before the real-time control experiments were conducted, two additional tests, a reference case and a base case test, were carried out. Both tests were required to calibrate the simulation model with respect to the building thermal response, the mechanical systems, and the operational schedules. Figure 5 shows the system configuration for the reference case and the base case. The active TES system is bypassed in the reference case.

4.1 Reference Case

The reference case represents the standard case of a cooling system with one sufficiently sized chiller (35 kW) which serves the air-handling units (AHU) A and B during occupancy, with nighttime setback during unoccupied periods and with neither active nor passive building thermal storage utilization. The test was run under the same schedule of occupancy and temperature setpoints: During occupied hours the zone temperature cooling setpoint was 24°C and the heating setpoint was 20°C, while the space temperature was allowed to float within the range of 15-30°C during unoccupied periods.

4.2 Base Case

In the base case test, the zone temperature setpoints were identical to the reference case test, however, the main chiller is downsized to only 25% of its nominal capacity (8.8 kW). During those periods when the cooling load exceeds the reduced chiller capacity, the remaining cooling is taken from the active TES system. At night the active TES system is recharged with full capacity of 35 kW to the upper inventory level of 75% state-of-charge. As in the reference case, the passive building thermal storage inventory is not utilized.

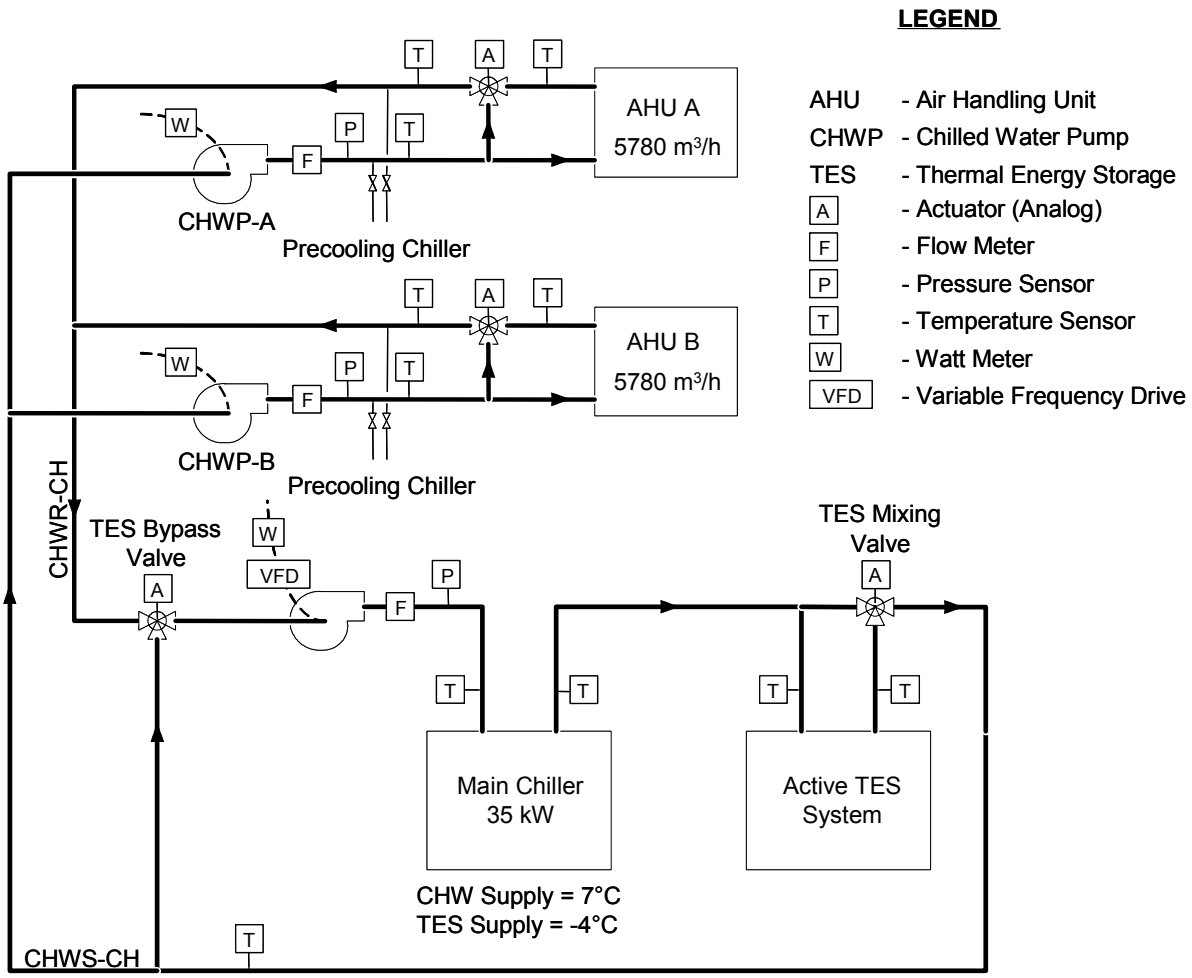

Figure 5: System schematic of ERS HVAC equipment

5 Results

5.1 Modeling Accuracy

The real-time optimal control experiment was executed over a period of 5 days (128 hours) from midnight on September 13 until 8 a.m. on September 18. In order to verify the experimental results, the accuracy of the building model must be evaluated. Minute-by-minute measurements taken at the test facility from September 14 to September 17, 2003 (subscript *ERS)* are compared to the optimal results determined by the controller during the real-time control experiment (subscript *ActPredOpt*, actual predictive optimal results). Preliminary tests conducted during June and July of 2003 facilitated the calibration the simulation model. As supported by evidence provided below, the accuracy of the building model was sufficiently high. Moreover, the post-processing program correctly translated and transferred the optimal control results and the HVAC systems and components were successfully orchestrated.

The experiment experienced two interruptions due to server crashes that made the communication channel to the building automation system unavailable on September 16 at 18:00 and on

September 17 at 12:00 noon. During these interruptions the BAS returned zero values for all properties and deviations between model and measured data necessarily occurred.

Figure 6 compares the total simulated and measured AHU cooling loads of system B. It can be seen that the measured and modeled values are in good agreement. However, there are some peak cooling loads which are not represented well by the model-based controller. The AHU loads are due to internal heat gains from baseboard heaters and lighting, which were chosen to be constant throughout the test days, solar gains, and the required intake of ventilation air.

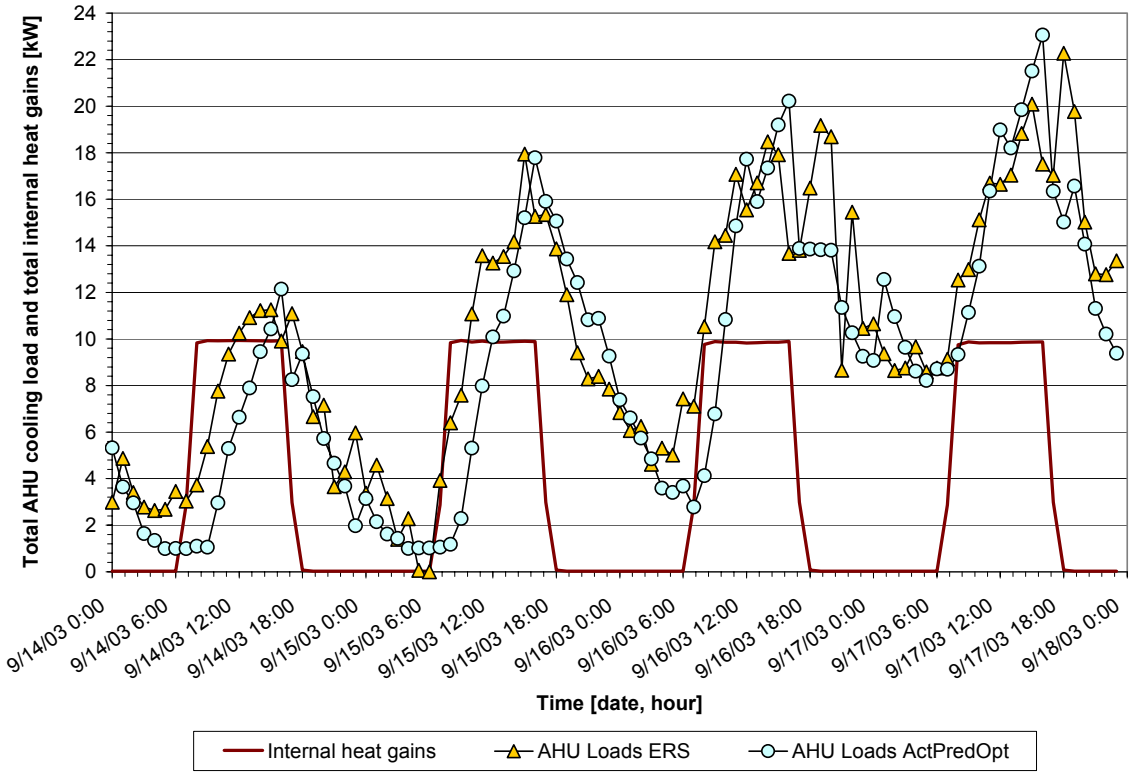

Figure 6: Measured and modeled total AHU cooling loads as well as measured internal heat gains [kW].

Figure 7 illustrates the measured and modeled charging and discharging performance of the active TES system for the September 15. It can be observed that the charging performance is accurately modeled; however, the discharge performance is modeled less precisely. Still, the discharge trend is captured well by the model used in the predictive optimal controller. While the charge/discharge performance appears to be adequately modeled, the profiles of the state-of-charge do not match well. Differences of up to 12% of active inventory can be observed and are attributed to a) the compounded differences in the charge/discharge performance and b) the poor accuracy of the inventory sensor (claimed to be ±5%). To eliminate the discrepancy between the simulated and measured values of state-of-charge, the SOC was measured throughout the testing period and updated seven times in the simulation environment. This procedure implies that the SOC sensor reads inventory levels accurately, which is not the case. Thus, the compounded effect of modeling mismatch in the charge/discharge process is eliminated, yet at the time the low SOC sensor accuracy is introduced to the optimization environment.

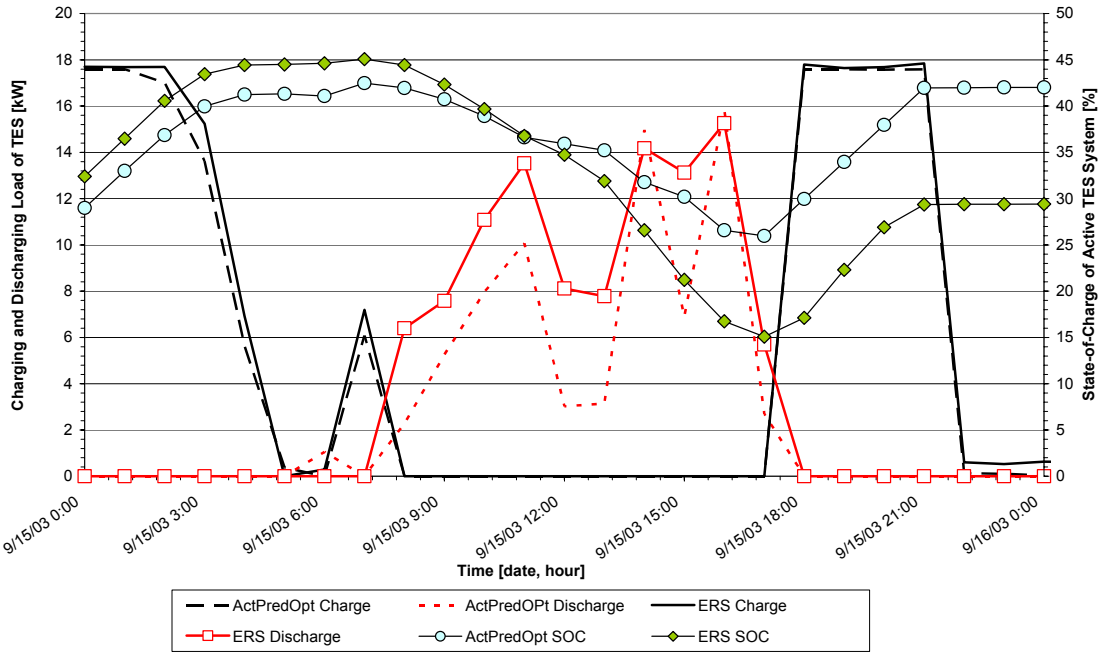

Figure 7: Measured and simulated charging and discharging load [kW] and state-of-charge [%].

Figure 8 illustrates the measured and simulated performance of the precooling chiller. Compared to the main chiller cooling profiles (not shown), the modeling accuracy for the precooling chiller is inferior. Unlike the active TES system and the main chiller, the precooling chiller was not controlled to maintain a particular value of $Q_{precool}$, but to maintain a global zone temperature setpoint $T_{Z,SP}$.

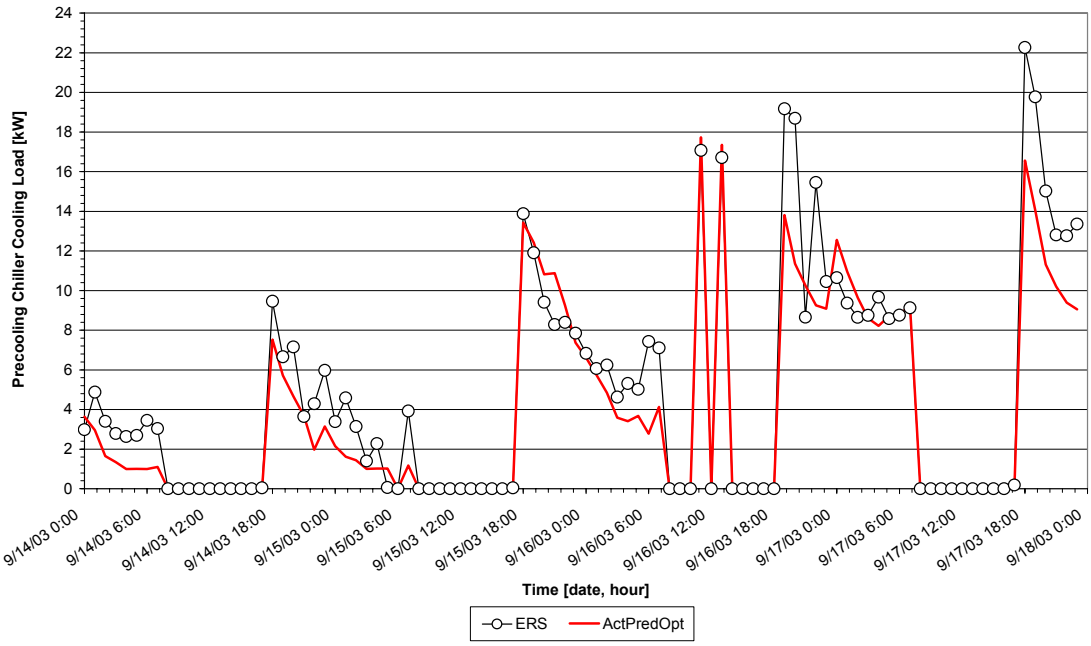

Figure 8: Measured and simulated precooling chiller cooling load [kW].

Does the model-based predictive optimal control comply with the operational constraints imposed in the model? Figure 9 shows the ambient air temperature, the average room air temperature, and the upper and lower temperature bounds selected for the operation of the ERS, represented by thick lines. During the real-time control experiment, the optimal controller decided on substantial nighttime precooling down to 20°C averaged over all test rooms. Had the controller decided to precool the building even lower, a need for heating would have occurred at the onset of the occupied period. When the temperatures were allowed to float as in the reference and base cases, the average test room temperature rises above 26°C during unoccupied periods. During occupied periods, the room temperature stayed within the required comfort range for all three control strategies investigated in this study.

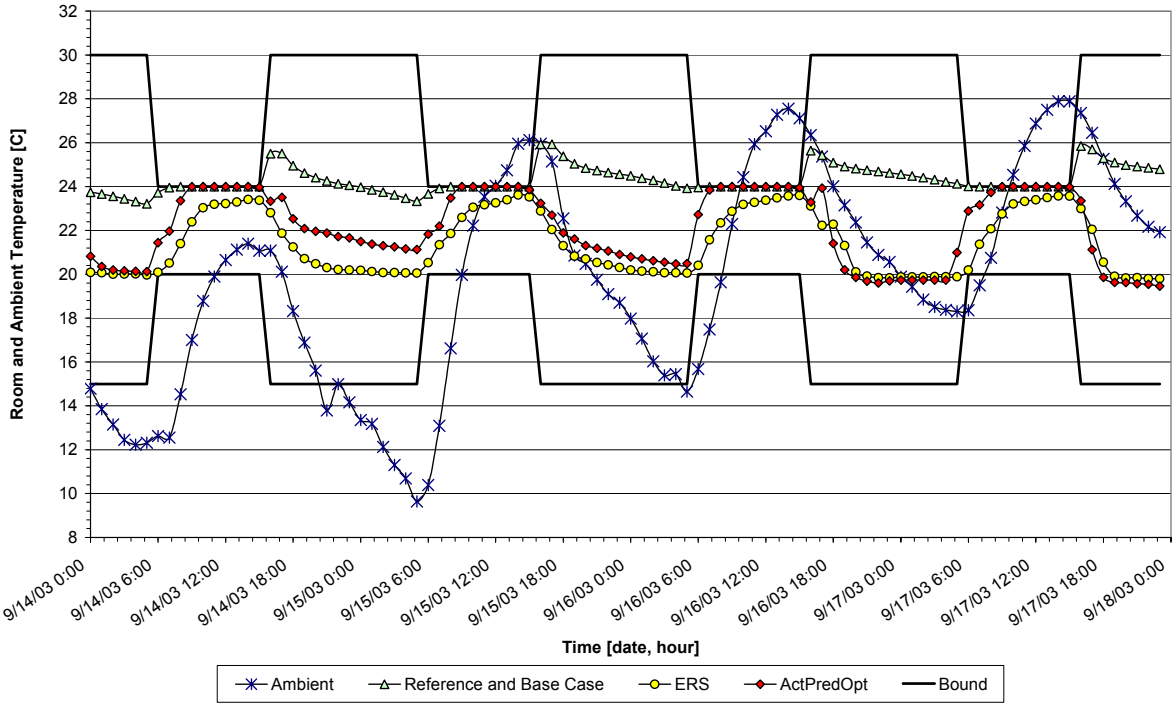

Figure 9: Average test room air temperature and ambient air temperature [°C].

The investigation of the active TES system state-of-charge data revealed that the simulated values remained consistently within the lower and upper bounds of 25% and 75%, respectively, while the measured TES inventory falls below the 25% mark due to a nonlinear discharging performance.

The average COPs of the main and precooling chillers were recalculated based on the data collected during the real-time control test in September of 2003. It was confirmed that the measured COPs deviated from the values in the building model by no more than ±0.1.

The schedules for occupancy and the HVAC system as implemented in the building model and the building automation system proved to match identically.

5.2 Energy and Cost Savings Performance

As mentioned above, changes in energy consumption and utility cost will be expressed relative to a simulated reference case or base case using the same building model and the same weather data as occurred during the real-time control tests. The performance metric for all cases is the utility cost for operating the entire HVAC system over a selected time horizon of

four days from September 14-17, 2003. The data for September 13 were not considered to account for the transition from the uncontrolled to the controlled condition.

5.2.1 Energy and Cost Savings Performance based on Raw Data

The electrical utility rate structure includes a time-of-use differentiated energy charges ($/kWh) of $0.20/kWh on-peak and $0.05/kWh off-peak; no demand charge is levied. The on-peak period is daily from 9 a.m. to 6 p.m. with off-peak encompassing all remaining hours. The building is occupied from 8 a.m. to 5 p.m. While the optimizer accounted reheat energy, no reheat was required in any of the test periods. The discussion therefore focuses on electrical energy consumption and costs.

The viewgraphs in this section are shown measurements at the ERS during the real-time-control test and simulation results for the reference and base cases for four days. In this time period, the outdoor air temperature ranges from 10°C early in the morning to 27°C at 6 p.m. Figure 9 reveals the increasing trend of daily average ambient air temperature over the course of the real-time control experiment.

In order to evaluate the results of the optimal control strategy with respect to cost and energy changes, the following tables and figures provide measured and calculated data for the following cases: a) reference case under nighttime setback, b) base case under chiller-priority control (labeled *Base Case 87%*), c) the data measured at the facility (labeled *ERS*), and d) the simulated data calculated during real-time control (labeled *ActPredOpt*). Both cases utilizing the active TES system, i.e., base and real-time control cases, started with an initial TES state-of-charge of 30%.

The original building model assumed a perfect, i.e., loss-free active TES system. This implies that 100% of the charging cooling load, Q_{charge}, is deposited in the storage tank. From measurements it was concluded that only about 87% of the cooling produced by the main chiller during the charging process contributes to changes of the active inventory storage, 13% are lost due to heat gains in the chilled-water distribution system and thermal transmission through the tank skin. For each charging period (5-7 hours per night) during the experiment, the change of the ice storage inventory was divided by the cumulative charging load that occurred over the same time period. The efficiency value of η = 87% was arrived at by averaging these five ratios.

$$\eta = \frac{1}{5}\sum_{p=1}^{5}\frac{\left(SOC_{final,p} - SOC_{inital,p}\right)}{\sum_{h=1}^{H_p} Q_{\text{charge},h,p}}, \tag{3}$$

where p denotes the charging period and H_p is the number of hours in charging period p. While the building model used for the ActPredOpt case assumed a perfect charging efficiency, the effect of heat gains and transmission losses on the state-of-charge was accounted for by periodically updating the SOC used in the simulation with measured SOC values at the test facility.

For an electrical utility rate structure without demand charges, we can plot daily profiles of HVAC utility costs for the main chiller, the precooling chiller, and chilled water pumps. The HVAC electrical energy consumption for September 17 is shown in Figure 10. The area under each curve represents the total daily operating consumption. It can be seen that the reference case incurs the highest on-peak demand, but as a result of nighttime setback does not consume any energy during the unoccupied period. The base case created the second highest energy demand during the on-peak period. Although the on-peak energy consumption for the base case is significantly less than that for the reference case, the on-peak consumption is greater than that under optimal control. During the day shown in Figure 10, the building cooling load

was moderate and only a small contribution from the active TES system was required in the base case. Consequently only four hours of recharging were needed.

The model-based predictive optimal controller successfully shifted building cooling loads to off-peak periods and an excellent match between calculated (ActPredOpt) and measured (ERS) cooling load data can be observed.

The simultaneous utilization of active and passive building thermal storage inventory led to near-zero cooling-related electrical energy consumption during the on-peak period. The remaining energy consumption during the on-peak period is caused by the chilled water pump operating continuously. During the off-peak period high values of energy consumption can be observed which are due to precooling of the building structure (passive) and charging of the active TES system. It is obvious that on-peak energy consumption is reduced at the expense of increased off-peak energy consumption driven by the energy rate ratio of 4:1. Reducing on-peak electrical demand is a side effect of shifting expensive on-peak cooling loads to off-peak periods for an optimal controller minimizing electrical energy cost without a demand charge.

Although the building model was extensively calibrated, the seemingly small differences between measured and modeled hourly HVAC electrical energy consumption compounded to significant differences on a daily basis.

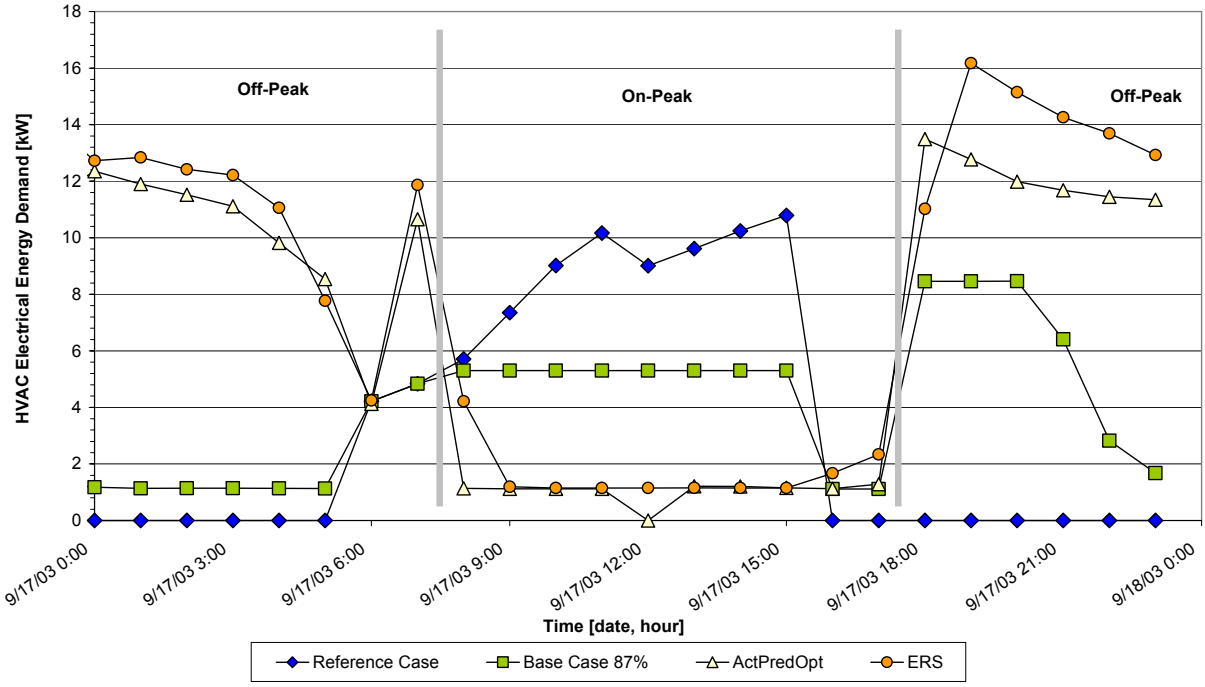

Figure 10: HVAC electrical energy consumption [kWh].

Table 1 provides the daily utility cost savings achieved during the experimental period. Relative to the reference case, measured savings of about 5% in total HVAC utility costs were achieved in the ERS, and about 10% of modeled savings (ActPredOpt). Compared to the base case with 87% charging efficiency, cost increases of about 7% and 1.4% were achieved for the ERS and the simulation, respectively. As shown, there are significant variations in the cost changes from one day to another relative to the reference and the base cases. This inconsistent pattern was caused by a number of reasons discussed in the next section.

Table 1: Changes of daily HVAC electrical utility cost of the optimal control strategy compared to the Reference Case and the Base Case 87% [%].

	14-Sep	15-Sep	16-Sep	17-Sep	Cumulative
Cost changes relative to Reference Case [%]					
ERS	-19.7	+11.5	+9.1	-21.2	-5.0
ActPredOpt	-32.2	+20.4	+7.1	-34.4	-9.9
Cost changes relative to Base Case 87% [%]					
ERS	-30.3	+17.3	+32.1	+1.3	+7.0
ActPredOpt	-41.1	+26.6	+29.7	-15.6	+1.4

5.2.2 Corrected Energy and Cost Saving Performance

Motivation for Correcting the Measured Results – Previous research (Henze et al., 2004a and 2004b) revealed that given strong load-shifting incentives, the benefits of the investigated predictive optimal control may be substantial. Therefore, we expected moderate daily savings, less fluctuation from day to day, and substantial cumulative savings. The promising potential of the optimal control strategy revealed in previous simulations may be obtained by the removal of erroneous data that occurred during the experiment. The corrected data discussed will be denoted by 'ERS*cor*' and 'ActPredOpt*cor*'.

Description of Experimental Problems – There were two experimental problems encountered during the tests: First, invalid data were produced by the building model during two hours of the experiment caused by the interruptions of the communication channel. These erroneous data were eliminated by interpolating between the valid adjacent data points.

Second, during three hours suboptimal solutions were found by the optimizer. As a result, main and precooling chiller activity occurred for three hours during the on-peak period of September 16 and drastically increased the electrical energy costs for that day. The precooling chiller activity can be observed for September 16 at 12 noon and 2 p.m. in Figure 8. The controller requested the main chiller to charge the TES with a very small charging load (not shown). As a result, the precooling chiller had to meet the daytime AHU cooling loads. Why did this happen? At any point in time, meeting a cooling load is least expensive by discharging the active TES system (only pump energy is incurred), next by using the precooling chiller (COP = 3.4), and finally by using the main chiller in chilled-water mode (COP = 2.1). Since both chillers cannot operate at the same time, the optimizer decided to charge an insignificant amount in order to be able to use the precooling chiller to meet the on-peak cooling loads. We believe that the optimal controller was caught in a local minimum during these hours, thus it selected a suboptimal control strategy. These experimental defects affected both the measured and the simulated raw cost data as shown in Table 1.

Elimination of Experimental Defects – In order to fairly assess the potential of the model-based predictive optimal controller, we manually modified the measured and simulated raw data to account for the interruptions and spurious precooling chiller activity. In addition, we repeated the experiment in a simulation environment using the same building model, weather data, and initial state-of-charge (labeled *RecPredOpt*), and compared it with the manually modified simulated data (labeled *ActPredOptcor*). The expectation was that after removing the experimental defects from the raw data and repeating the simulation without the problem of local minima, the results should match closely. Indeed, a repeated simulation run did not produce the same idiosyncrasies with respect to the precooling chiller operation as can be seen in Figure 12.

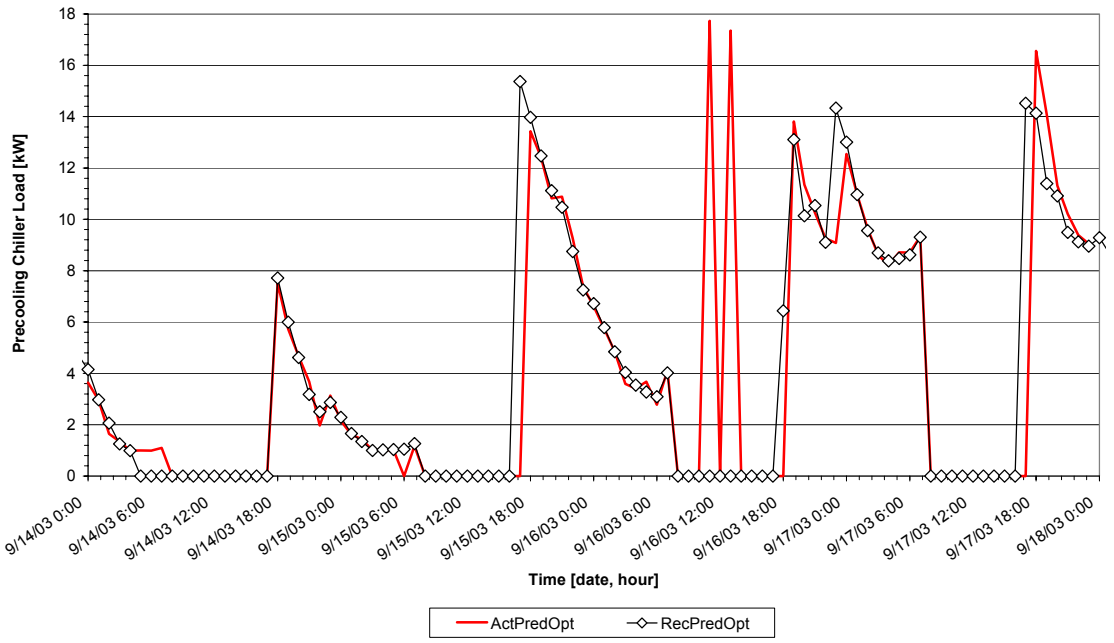

Figure 11: Simulated precooling chiller load as determined during the real-time experiment (Act-PredOpt) and during recreated experiment (RecPredOpt) [kW].

The recreated experiment determines the cost savings we may have had obtained without interruptions and local minima. Interestingly, there are minor differences between the results collected for the real-time optimization ActPredOpt*cor* and the recreated optimization RecPredOpt. Obviously, the controller does not find exactly the same optimal solutions, which can be attributed to the convergence criterion of the optimizer.

Cost Comparison using the Modified Measured Results and the Recreated Simulation – Table 2 compares the daily savings of the corrected measurements at the ERS and of the corrected real-time simulation with the reference and base cases. It can be seen that the values for September 16 and 17 differ greatly from the cost calculation involving the raw data as shown in Table 1. After the removal of the erroneous data we obtain cost savings of 13% for the ERS data compared to the reference case and savings of 2% relative to the base case. The corrected real-time optimal results reveal higher cost savings as well. Cumulative savings of 18% are obtained when compared to the reference case and 7% are obtained relative to the base case. When comparing the recreated optimal results without local minima complications against the reference case, we obtain the same 18% savings as for corrected simulation results.

The recreated simulation did not require any updates of the SOC values since it did not occur in real-time and actual SOC data was not available. In order for the comparison of the recreated optimal and simulated base case to be valid, both have to use the same active TES model. We decided to assume a perfectly efficient charging process in the TES system for this comparison. The comparison yielded cost savings of about 7%.

Table 2: Changes of daily corrected HVAC electrical utility cost of the optimal control strategy compared to the Reference Case and the Base Case [%].

	14-Sep	15-Sep	16-Sep	17-Sep	Cumulative
Cost changes relative to Reference Case [%]					
ERS*cor*	-19.7	+11.6	-19.0	-22.4	-13.6
ActPredOpt*cor*	-32.8	+19.8	-19.6	-34.3	-18.0
RecPredOpt	-35.3	+13.2	-18.2	-30.5	-18.2
Cost changes relative to Base Case 87% [%]					
ERS*cor*	-30.2	+17.4	-1.9	+1.2	-2.2
ActPredOpt*cor*	-41.7	+26.0	-2.6	-14.2	-7.2
Cost changes relative to Base Case 100% [%]					
RecPredOpt	-42.9	+19.0	0	-8.3	-6.6

5.2.3 Consideration of AHU Fan Power Consumption

Motivation for Neglecting AHU Fan Operation – Preliminary tests had revealed that the global optimization of both active and passive building thermal storage inventory led to prohibitively long calculation times and inferior, i.e., often suboptimal solutions. In response, we adopted the iterative sequential optimization approach depicted in Figure 3. This decision required the plant models of the passive and active optimization steps are identical. To allow for easy plant model calibration, we decided to include a simplified HVAC plant model characterized by constant COPs in each mode of operation excluding the operation and energy consumption of the fans.

The measured data revealed that the fan energy consumption cannot be neglected and that fan operation has a significant impact on the decisions of the model-based predictive optimal controller. Therefore, the discussion of energy consumption and cost performance is now extended to take into account the fan power consumption and to highlight the differences in the optimal control decisions with and without fans.

Results with AHU Fan Power Consumption – On the basis of measured data, we approximated the supply and return fan electrical power consumption for AHU A and B with second-order polynomials and integrated those in the building model. The simulated results, shown in Figure 12 below, present the hourly HVAC electrical demand on September 17 for the reference case, the base case, the corrected measured data ERS*cor*, and the repeated optimal results RecPredOpt. The energy required by the reference case and the base case increased by the energy consumption of the fans during the occupied period.

Using the new plant model, the optimizer in a recreated experiment decides to make less use of the passive building thermal storage inventory, i.e., less precooling during the night and as a result saves an impressive 27% and 17% of electrical utility costs relative to the reference and base cases, respectively.

The actual experiment was conducted governed by a model-based predictive optimal controller that did not account for AHU fan power consumption. If we compare the measured total HVAC electrical energy consumption ERS*cor* with the fan consumption added to the reference and base cases using the modified plant model, the savings are reduced from 13.6% to 5.6% for the reference case and from 2.2% savings to cost increases of 8.3%. This investigation emphasizes that the inclusion of fan power consumption is mandatory for a successful implementation of passive thermal storage utilization. The optimal active TES system control strategy was not materially affected by the inclusion of the AHU fans in the plant model.

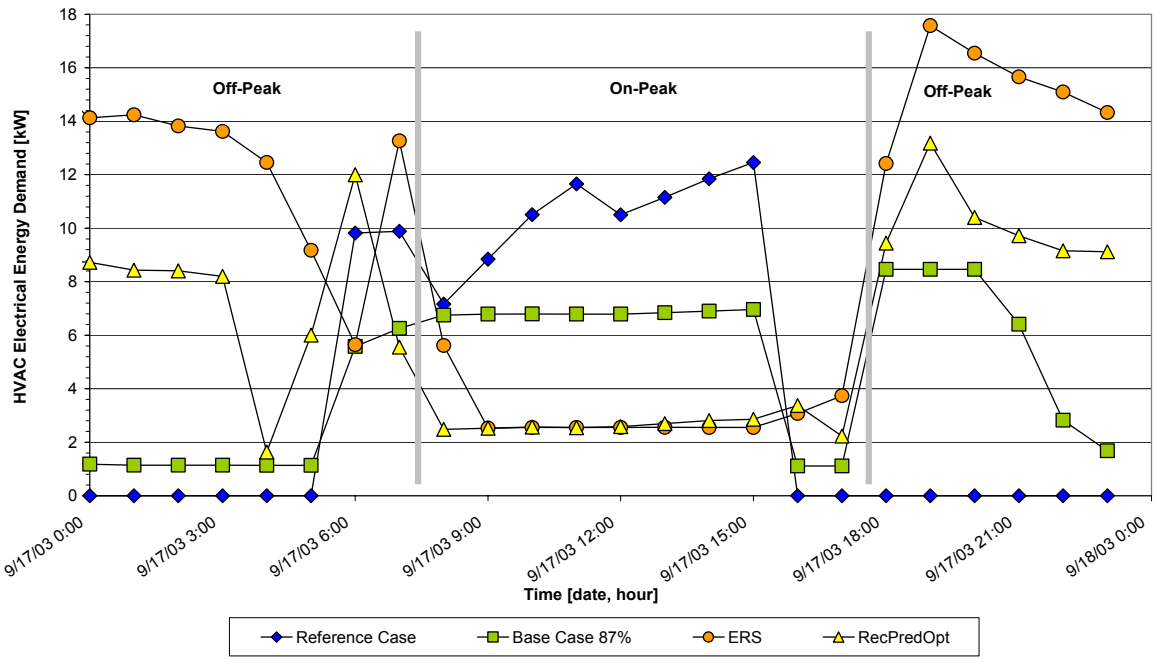

Figure 12: HVAC electrical demand including fan operation [kW].

Table 3: Changes of daily corrected HVAC electrical utility cost of the optimal control strategy compared to the Reference Case and the Base Case including the fan power consumption [%].

	14-Sep	15-Sep	16-Sep	17-Sep	Cumulative
Cost changes compared to the Reference Case [%]					
ERS*cor*	-7.9	+13.5	-11.4	-13.2	-5.6
RecPredOpt	-30.0	-13.9	-26.4	-36.4	-27.3
Cost changes compared to Base Case 87% [%]					
ERS*cor*	-11.6	+25.4	+7.5	+9.6	+8.3
Cost changes compared to Base Case 100% [%]					
RecPredOpt	-32.9	-4.9	-10.7	-19.8	-16.7

6 Conclusions and Future Work

This topical report investigates the demonstration of model-based predictive optimal control for active and passive building thermal storage inventory in a test facility in real-time using time-of-use differentiated electricity prices without demand charges. The novel supervisory controller successfully executed a three-step procedure consisting of 1) short-term weather prediction, 2) optimization of control strategy over the next planning horizon using a calibrated building model, and 3) post-processing of the optimal strategy to yield a control command for the current time step that can be executed in the test facility.

The primary and secondary building mechanical systems consisting of two air cooled chillers, an ice-based thermal energy storage system, two identical air handling units and auxiliary equip-

ment were effectively orchestrated by the model-based predictive optimal controller in real-time while observing comfort and operational constraints. The authors believe that this has not been accomplished before.

The findings reveal that when the optimal controller is given imperfect weather forecasts and when the building model used for planning control strategies does not match the actual building perfectly, measured utility costs savings relative to conventional building operation can be substantial. This requires that the facility under control lends itself to passive storage utilization and the building model includes a realistic plant model.

The savings associated with passive building thermal storage inventory proved to be small because the test facility is not an ideal candidate for the investigated control technology: The building structure is of light-weight construction, the test rooms are unfurnished, and significant thermal coupling exists between controlled test rooms and an uncontrolled adjacent area. Moreover, the facility's central plant revealed the idiosyncratic behavior that the chiller operation in the ice-making mode was more energy efficient (COP=2.4) than in the chilled-water mode (COP=2.1).

To aid model calibration, the model used for real-time control employed a constant COP approach for each chiller and mode of operation and ignored VAV fan operation. The measured results show that the plant model must include AHU fan operation and should include part-load performance and correction for off-design conditions.

Field experimentation is now required in a suitable commercial building with sufficient thermal mass, an active TES system, and a climate conducive to passive storage utilization over a longer testing period to support the laboratory findings presented in this study.

Currently underway is research that attempts to create an optimal controller for the same control application that does not rely on a model description but learns to carry out the best control decisions based on reinforcement it received in response to past actions.

7 Acknowledgement

The authors gratefully acknowledge the financial support of this work through U.S. Department of Energy Cooperative Agreement No. DE-FC26-01NT41255 and the outstanding on-site technical support at the Energy Resource Station of the Iowa Energy Center provided by Curtis Klaassen, Xiaohui Zhou, and David Perry.

8 References

American Refrigeration Institute (ARI) (1999) Statistical Profile of the Air-Conditioning, Refrigeration, and Heating Industry. p. 28, Arlington, VA.

American Standard, Inc. (1999) *EarthWise Today*, Vol. 24, p. 3. LaCrosse, Wisconsin.

Arthur D. Little, Inc. (1999) *Guide for Evaluation of Energy Savings Potential*. Prepared for the Office of Building Technology, State and Community Programs (BTS), U.S. Department of Energy.

Braun J.E., T.M. Lawrence, C.J. Klaassen, and J.M. House (2002) "Demonstration of Load Shifting and Peak Load Reduction with Control of Building Thermal Mass," *Proceedings of the 2002 ACEEE Conference on Energy Efficiency in Buildings*, Monterey, CA.

Braun, J.E. (2003) "Load Control Using Building Thermal Mass", *Journal of Solar Energy Engineering*, Vol. 125, No. 3, pp. 292-301, American Society of Mechanical Engineers, New York, New York.

Energy Information Administration (EIA/DOE) (2002) *Annual Energy Review 2002*. U.S. Department of Energy. URL: http://www.eia.doe.gov/emeu/aer/enduse.html. October 2003.

National Energy Technology Laboratory (NETL/DOE) (2003) *Federal Assistance Solicitation for Energy Efficient Building Equipment and Envelope Technologies Round IV.* PS No. DE-PS26-03NT41635. p. 4. U.S. Department of Energy.

Henze, G.P., R.H. Dodier, and M. Krarti (1997) "Development of a Predictive Optimal Controller for Thermal Energy Storage Systems." International Journal of HVAC&R Research, Vol. 3, No. 3, pp. 233-264.

Henze, G.P., C. Felsmann, and G. Knabe (2004a) "Evaluation of Optimal Control for Active and Passive Building Thermal Storage." *International Journal of Thermal Sciences*, February 2004.

Henze, G.P., D. Kalz, C. Felsmann, and G. Knabe (2004b) "Impact of Forecasting Accuracy on Predictive Optimal Control of Active and Passive Building Thermal Storage Inventory." April 2004. *International Journal of HVAC&R Research*.

Liu, S. and G.P. Henze (2004) "Impact of Modeling Accuracy on Predictive Optimal Control of Active and Passive Building Thermal Storage Inventory." *ASHRAE Transactions*, Technical Paper No. 4683. Vol. 110, Part 1.

Matlab (2000) Using Matlab v6. The MathWorks, Inc.

Price, A.B. and T. F. Smith (2000) "Description of the Iowa Energy Center Resource Station: Facility Update III", Technical Report ME-TFS-00-001, Department of Mechanical Engineering, The University of Iowa, Iowa City.

TRNSYS (2003) TRNSYS – A transient simulation program. SEL University of Wisconsin – Madison, http://sel.me.wisc.edu/trnsys/Default.htm.

9 Nomenclature

AHU	Air handling unit
ActPredOpt	Raw actual predictive optimal results during real-time simulation
ActPredOptcor	Corrected predictive optimal results during real-time simulation
BAS	Building automation system
Base Case 87%	Base case under chiller priority with 87% charging efficiency
Base Case 100%	Base case under chiller priority with 100% charging efficiency
CHWP	Chilled water pump
CLO	Closed-loop optimization
COP	Coefficient-of-performance
ERS	Energy Resource Station; raw measured data at ERS
ERScor	Corrected measured data at ERS
IEC	Iowa Energy Center
HVAC	Heating, ventilating, and air-conditioning
PWM	Pulse width modulation

RecPredOpt	Repeated predictive optimal results
SOC	State-of-charge for the inventory in the active thermal storage system [%]
TES	Active thermal energy storage system
TESACC	Plant mode: Condition the test rooms
TESACCOFF	Plant mode: Turn off HVAC system
TESMAKE	Plant mode: Charge active TES system
VFD	Variable-flow distribution
C_L	Cost function for horizon *L* [$]
C_m	Total monthly utility bill [$]
H_p	Number of hours in charging period *p* [-]
J_m	Optimal total monthly utility bill [$]
J_L	Optimal utility cost for horizon *L* [$]
K_m	Number of hours in current month [-]
L	Planning horizon for optimal control [h]
Q_{charge}	Charging load for the main chiller [kW]
$Q_{discharge}$	Discharging load for TES system [kW]
Q_{heat}	Heating demand from zone reheat [kW]
Q_{main}	Cooling load for main chiller [kW]
$Q_{precool}$	Cooling load for precooling chiller [kW]
$T_{EW,TES}$	Entering water temperature of TES [°C]
$T_{LW,TES}$	Leaving water temperature of TES [°C]
$T_{z,SP}$	Global zone temperature setpoint [°C]
$\left\{\hat{X}_t\right\}$	Forecasted time series
$\left\{X_t\right\}$	Observed time series
c_p	Specific heat capacitance [kJ/kgK]
d	Number of days [-]
k^*	Current hour [-]
$\dot{m}$	Mass flow rate [kg/s]
n	Day index [-]
$r_{e,k}$	Energy rate for electricity [$/kWh]
r_h	Cost of heat delivered [$/kWh]
t	Time [-]
u	Charge/Discharge rate [-]
Δt_h	Time increment for one hour [-]
η	Efficiency value for charging TES [%]

Appendix – Additional Tests at the Larson HVAC Laboratory

10 Description of the Larson HVAC Laboratory

The Larson Building System Laboratory at the University of Colorado at Boulder shown in Figure 13 is a unique facility in the HVAC industry in that it permits the study of entire HVAC systems in a controlled dynamic environment, providing repeatable test conditions that have been heretofore unavailable. It is used for educational and research purposes and is designed for dynamic testing of complete and full-scale commercial HVAC and building systems. The facility consists of a full-size commercial HVAC system, four representative commercial building zones, a system for producing repeatable and controllable loads on the HVAC system, and sophisticated data acquisition and control systems. Activities at the laboratory include evaluation and testing of control algorithms and hardware for HVAC components and systems, interactions between multiple control functions of HVAC systems, the dynamic interactions between building thermal response and HVAC system controls, ventilation control for indoor air quality, and HVAC system diagnostics.

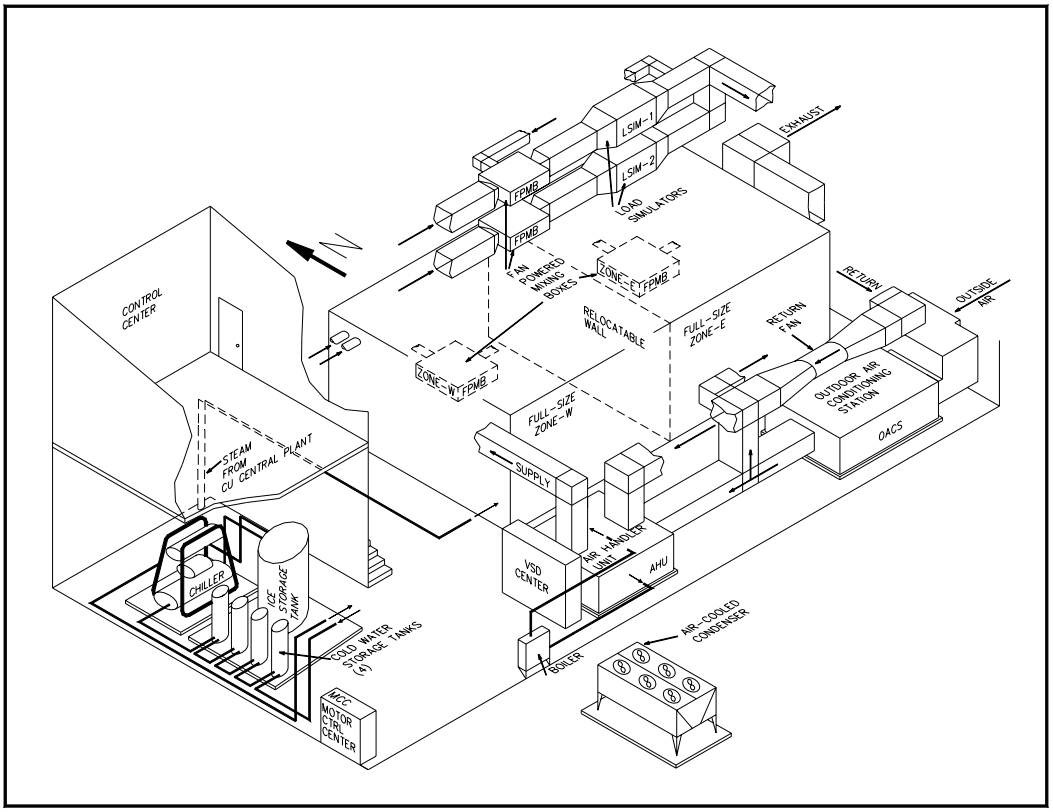

Figure 13: Isometric View of Larson Laboratory at the University of Colorado

The laboratory has been designed for maximum flexibility to encourage a wide variety of research and testing programs. In particular, both the HVAC and control systems in the laboratory are re-configurable in that components, subsystems or entire systems can be readily installed, tested, and modified.

The main HVAC system of the laboratory consists of a 12,000 cfm air-handling unit that is connected to four building zones by variable-air-volume (VAV) fan powered mixing boxes. To pro-

vide cooling to the four zones, a chiller, rated at 265 kW (75 tons) cooling capacity comprised of two screw-type compressors, is available within the lab. Continuous capacity control is provided down to 10% of rated capacity. This chiller, a 2.2 kW (3 hp) constant-volume pump, and a 668 kWh (190 ton-hour) ice storage tank are incorporated into a primary loop. A separate constant-volume 2.2 kW (3 hp) pump circulates water through a secondary loop to the zone simulators and the two air-handling units. The chilled water loop contains 25% glycol brine and allows the primary loop to operate at temperatures as low as -5°C. The ice storage tank will be used to provide chilled water to the air-handling unit.

The entire lab is controlled using programmable direct digital control (DDC). The DDC system uses electronic actuators for damper and valve control, all of which accept standard analog control signals. The system employs laboratory-grade instrumentation for accurate control. All the control strategies to be tested in this project can be easily programmed using this DDC system. The data acquisition can accommodate up to 300 data channels. Data collected include temperature, humidity, pressure, flow rate, fan speed, and electric power consumption. The accuracy measurements meet or exceed all relevant ASHRAE/ASTM standards.

11 Description of the Experiments

The experiments focus on lab validation of optimal control of active and passive building thermal storage inventory in a light-mass building as represented by the Larson HVAC Laboratory at the University of Colorado at Boulder.

Experiments on passive-only, active-only and combined building thermal storage control were carried out and the results analyzed. Two electrical utility rates are studied: a strong incentive rate and a weak incentive rate. For the strong incentive rate, on-peak and off-peak energy charges are 0.20 $/kWh and 0.05 $/kWh respectively and demand charges are 20 $/kW and 5 $/kW respectively. In the weak incentive rate, on-peak and off-peak energy charges are 0.10 $/kWh and 0.05 $/kWh respectively and demand charges are 10 $/kW and 5 $/kW respectively. The results from experiment and simulation are discussed below.

11.1 Base Case

The building is occupied from 8:00-19:00, the on-peak period is 10:00-18:00 and the rest of the day is off-peak period. The two zone simulators (ZSIM1, ZSIM2) are conditioned to 75°F for 24 hours with internal loads schedules of 19 kW and 20 kW for 24 hours respectively. The two full size zones (FSZW, FSZE) are conditioned to 75°F during occupied period and allowed to float up to 105°F during unoccupied period. The peak internal loads of the two full size zones are 6 kW each zone. The internal loads are 30% peak load during 8:00-9:00, 12:00-13:00 and 18:00-19:00 and 50% peak load during 9:00-12:00 and 13:00-18:00. Simulated weather file of summer design day in Phoenix, AZ are successfully incorporated in the outside air conditioning station (OACS) as illustrated by Figure 14.

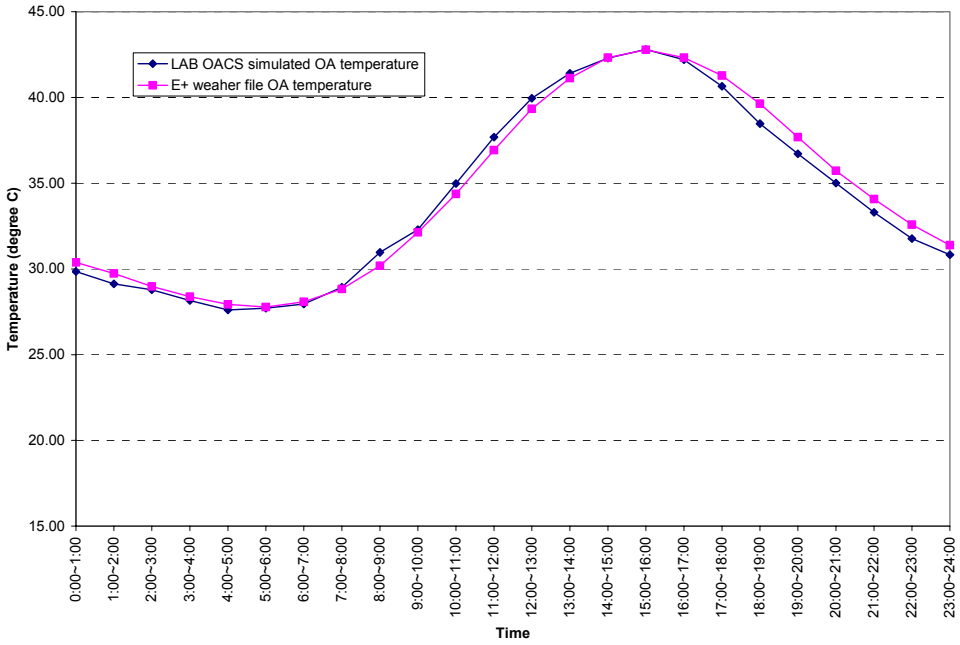

Figure 14: Simulation and measured outdoor air dry-bulb temperature profiles

Figure 15 shows the indoor air temperatures, and chiller power consumption profile comparison between experiment and simulation results. Excellent agreement between model and laboratory performance can be noted. The average error of simulation on chiller power consumption is 0.6%.

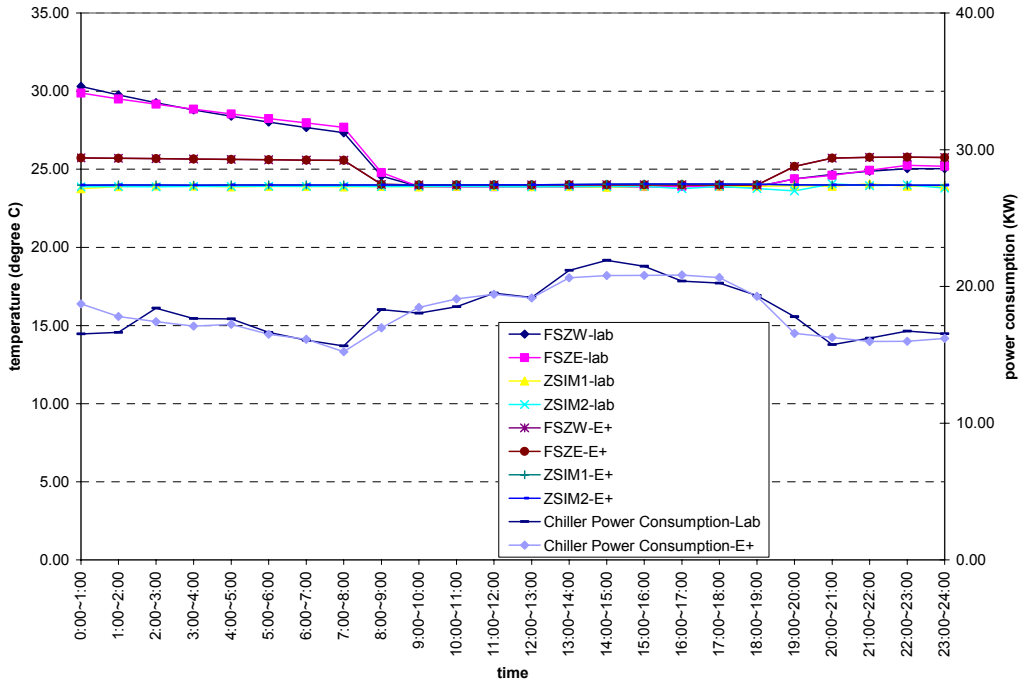

Figure 15: Simulated and measured zone air temperature and chiller power consumption profiles under base case control

11.2 Strong Incentive Utility Rate

11.2.1 Passive-Only (Nighttime Precooling)

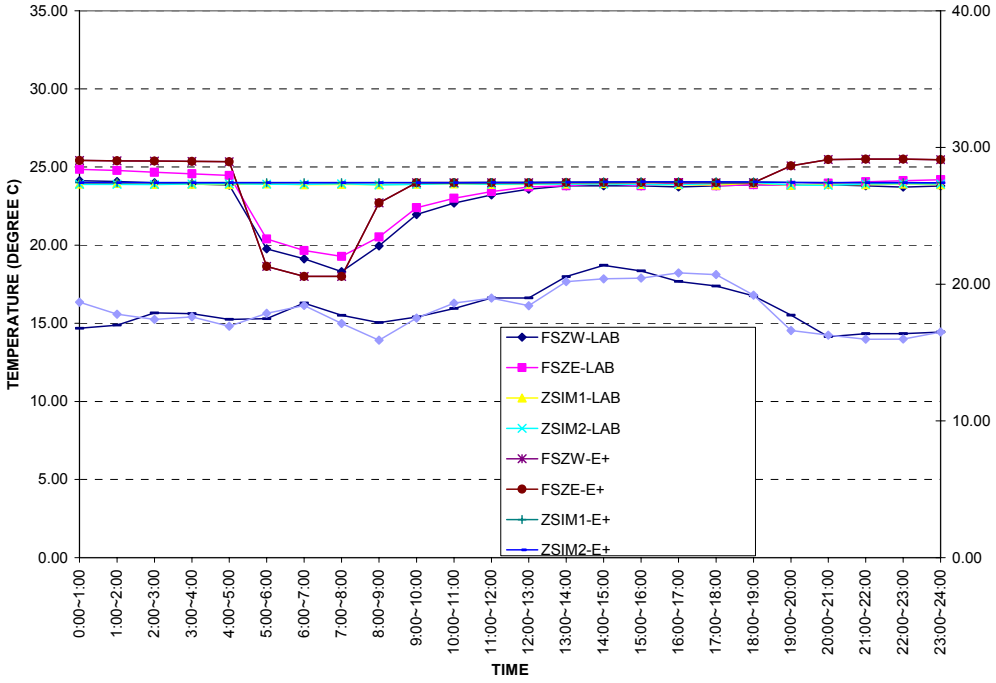

Figure 16: Simulated and measured zone air temperature and chiller power consumption profiles in passive-only optimal control under strong incentive utility rate

The optimal passive building thermal storage control suggests precooling the full-size zones to 18.3°C for 3 hours before occupancy then maintaining zone setpoint of 24°C. In the experiment and as expected, it is found that the zone temperature of the full-size zones does not drop to 18.3°C immediately. It takes about 2 hours to cool the zone to desired precooling temperature. Also, after precooling, the zone temperature rise more slowly than the simulation results. In general, the difference in chiller power consumption between experiment and simulation are within an acceptable range. The chiller consumes more power during 5:00-8:00 due to precooling and cooling energy costs are slightly lower than the base case.

11.2.2 Active-Only (Ice Storage)

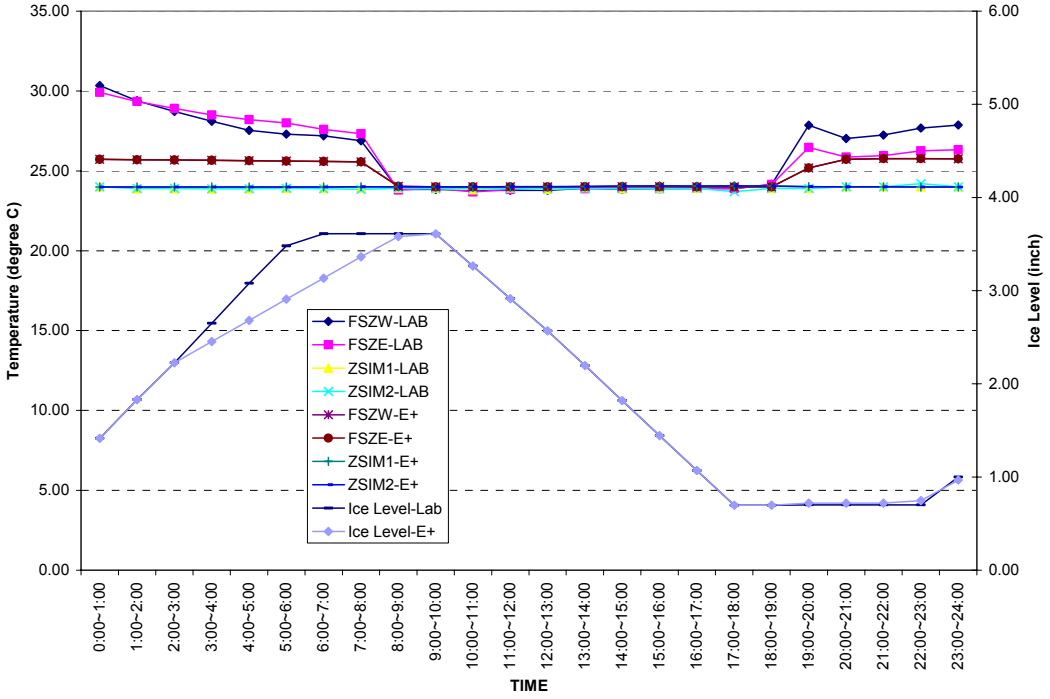

Figure 17: Simulated and measured zone air temperature and TES state-of-charge profiles of active-only optimal control under strong incentive utility rate.

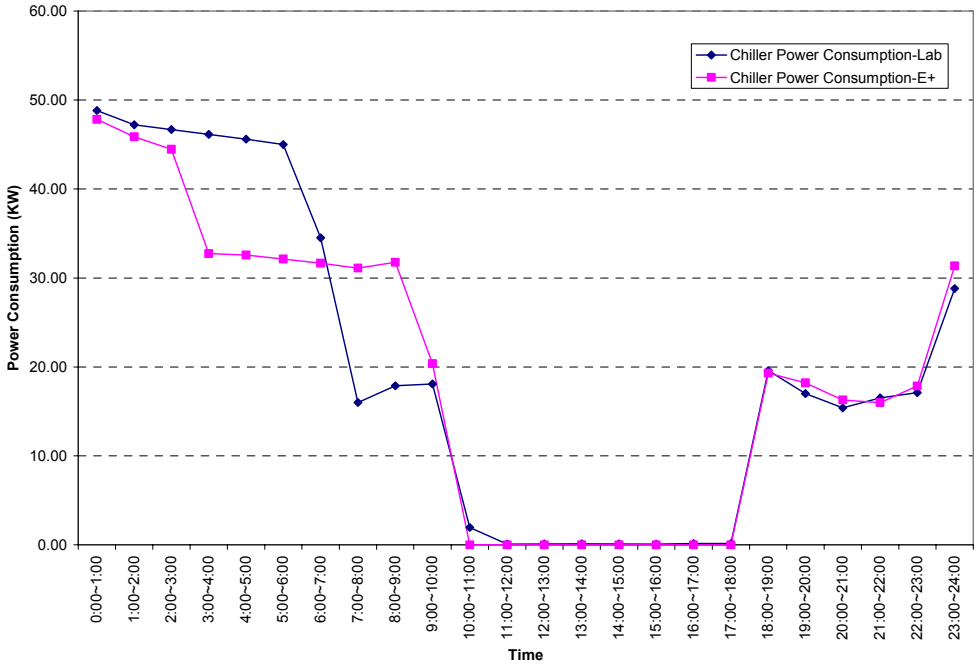

Figure 18: Simulated and measured chiller power consumption profiles in active-only optimal control under strong incentive utility rate

From Figure 17 and Figure 18, it can be observed that the simulated and measured TES state-of-charge profiles and chiller power consumption profiles display differences. This is due to the difficulty of controlling the TES charging process as accurately as the simulation because of the existence of constant speed pump and PID controlled valve as well as the nonlinear heat transfer characteristics of the active storage itself. In the experiment, only the initial and final ice level during charging and discharging process is controlled. Although the profiles reveal differences, the error of total power consumption and energy cost are 3% and 8%, respectively, and deemed as acceptable.

11.2.3 Combined Active and Passive Building Thermal Storage

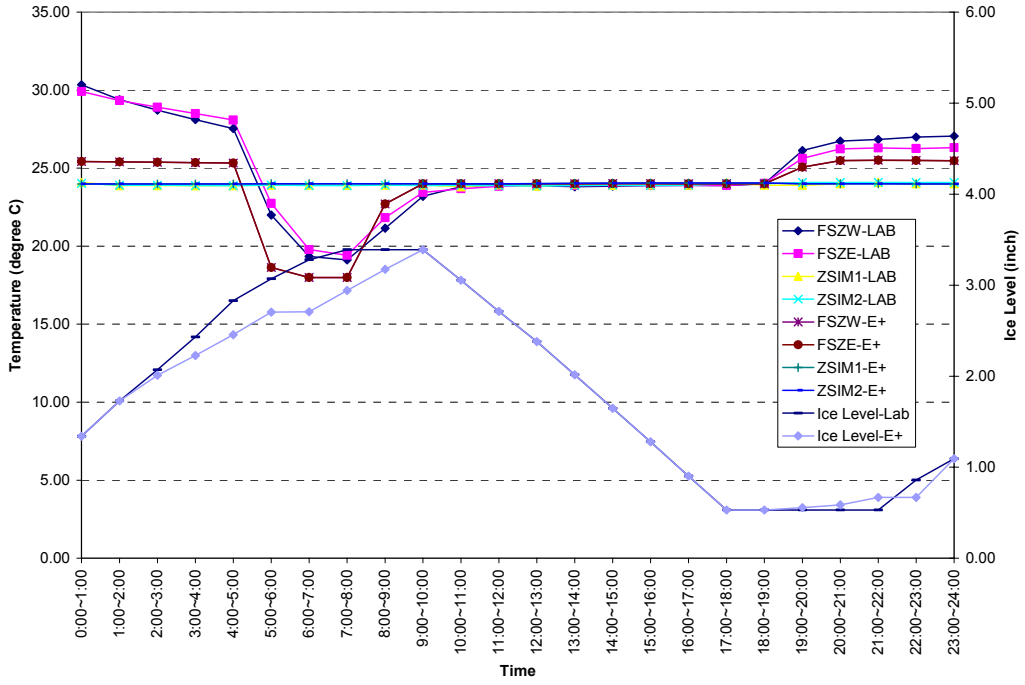

Figure 19: Simulated and measured zone air temperature and TES state-of-charge profiles in combined active and passive optimal control under strong incentive utility rate

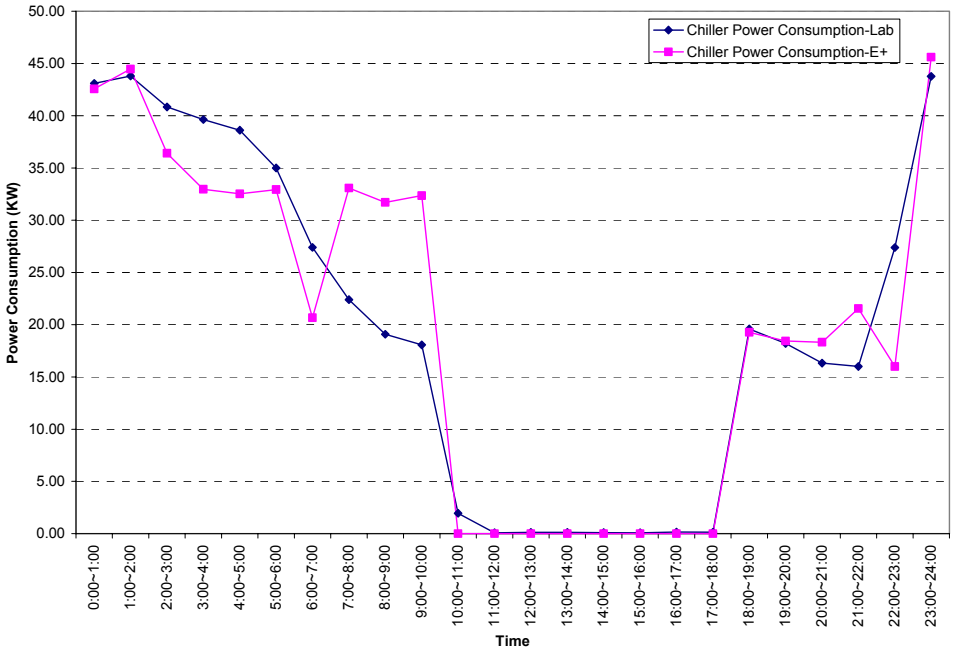

Figure 20: Simulated and measured chiller power consumption profiles in combined active and passive optimal control under strong incentive utility rate

The passive building thermal storage inventory is precooled to 18°C for 3 hours before occupancy and the ice tank is charged to from 1" to 3.4" inches of ice before the beginning of the on-peak period and discharged to 0.53" during the on-peak time and after that recharged to 1". The error of total chiller power consumption and energy costs are 1% and 3%, respectively.

11.3 Weak Incentive Utility Rate

11.3.1 Passive-Only (Nighttime Precooling)

The optimal control of passive building thermal storage under weak rate ratio is the same as that of intensive rate ratio in our case. Only the percentage of savings achieved is reduced. The error of total power consumption and energy costs are within 1%.

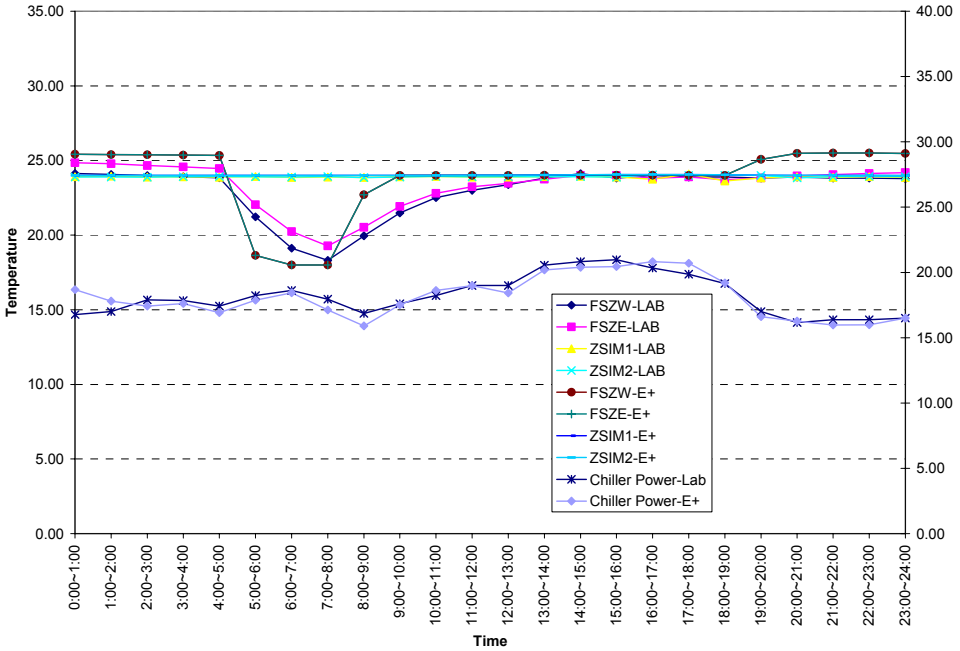

Figure 21: Simulated and measured zone air temperature profiles and chiller power consumption in passive-only optimal control under weak incentive utility rate

11.3.2 Active-Only (Ice Storage)

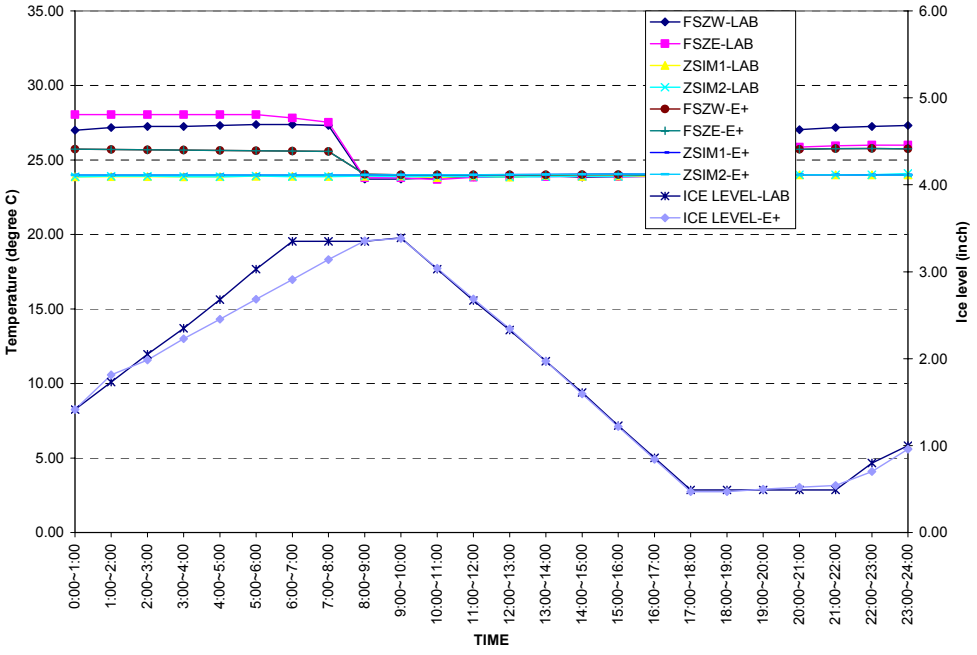

Figure 22: Simulated and measured zone air temperature and TES state-of-charge profiles in active-only optimal control under weak incentive utility rate

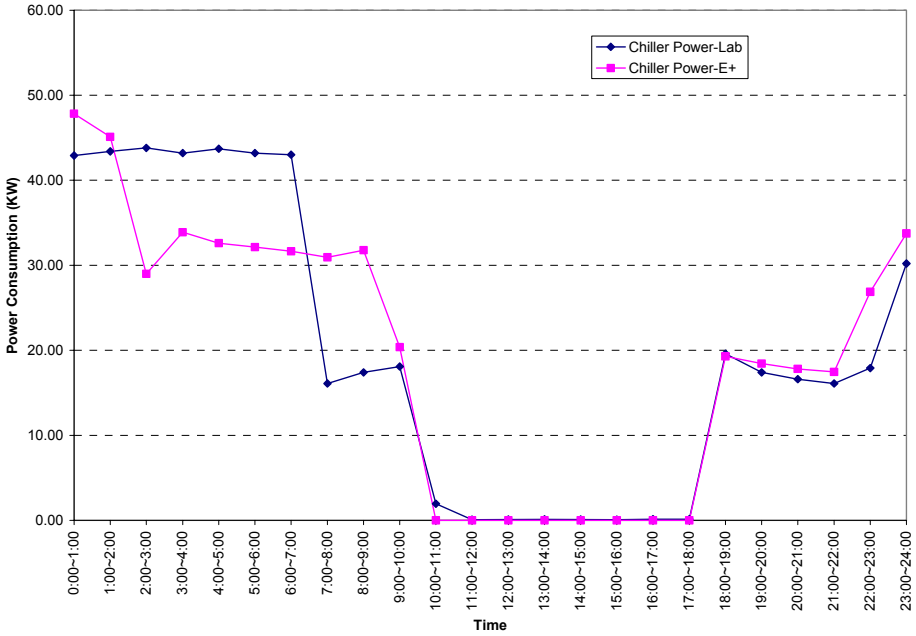

Figure 23: Simulated and measured chiller power consumption profiles in active-only optimal control under weak incentive utility rate

The ice tank is charged from 1" to 3.39" of ice level before occupancy and discharged to 0.5" of ice level during on-peak time and recharged to 1" in the night. The error of cost savings is within 1%.

11.3.3 Combined Active and Passive Building Thermal Storage

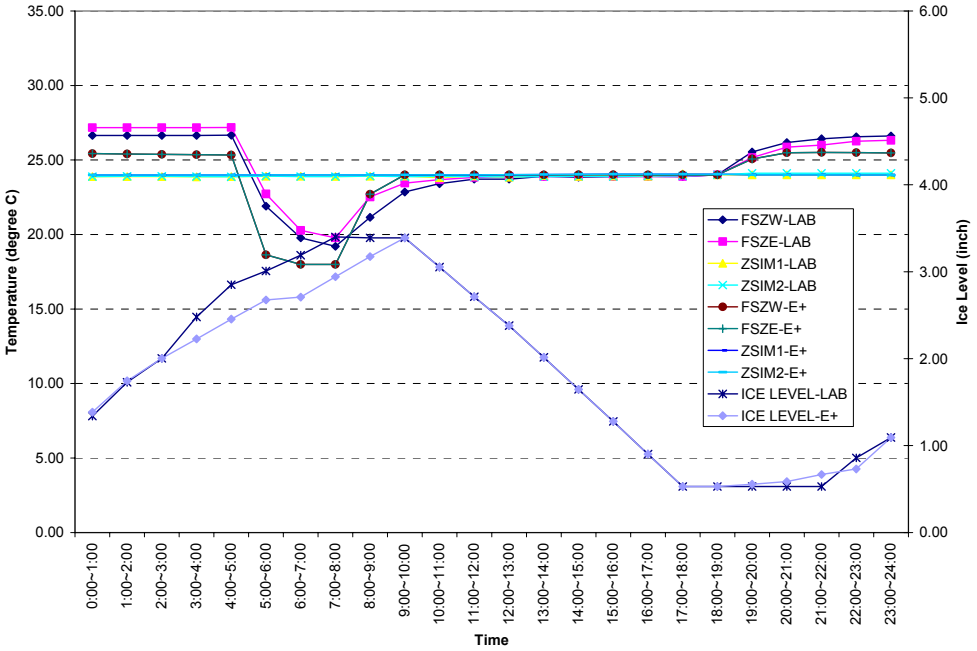

Figure 24: Simulated and measured zone air temperature and TES state-of-charge profiles in combined-TES optimal control under weak incentive utility rate

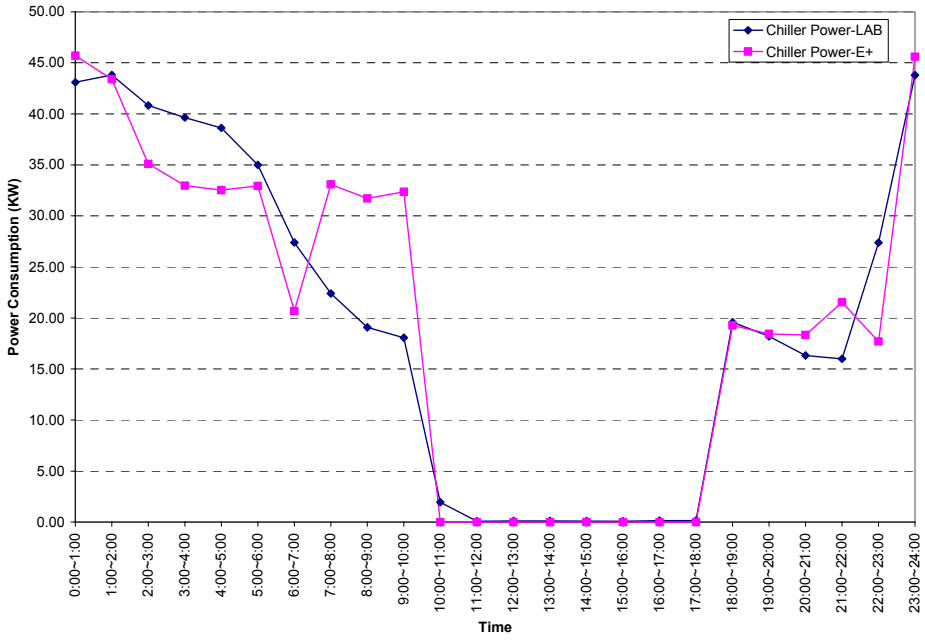

Figure 25: Simulated and measured chiller power consumption profiles in combined active and passive building thermal storage optimal control under weak incentive utility rate

11.4 Effect of night floating temperature in full size zones.

As can be seen from the previous figures, in some of the experiment, the nighttime floating temperature of the full size zones is different from that from simulation. This is mainly due to the fact that in some of the experiment, the lights in the full size zones are kept on during the night. In the morning, different zone temperature will affect the results of optimization.

Therefore, simulations were conducted to study the impact of nighttime zone floating temperature on optimization results. Figure 13 shows the zone temperature profiles and chiller power consumptions in two optimal controls with different initial zone temperatures. Table 1 shows the comparison of cost savings achieve under high and low initial temperatures.

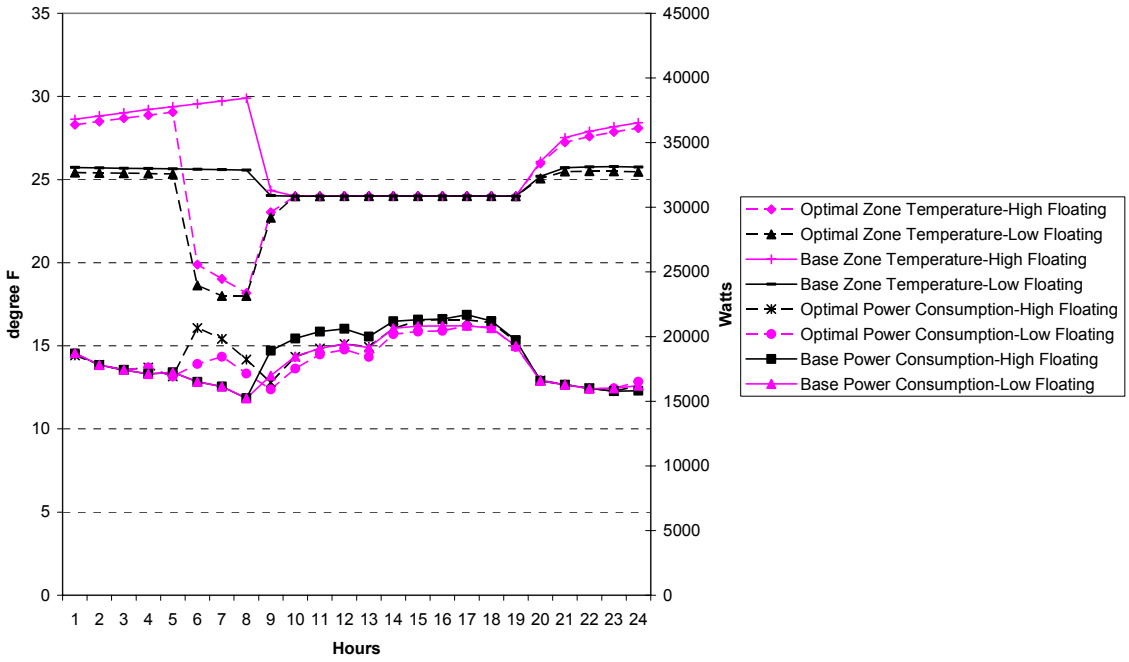

Figure 26: Zone temperature and chiller power consumption profiles under different nighttime floating temperatures for light mass with strong incentive utility rates.

Table 4: Comparison of Cost Saving Achieved by Optimal Control of Passive TES under High and Low Floating Temperature

		Hight Floating Temperature	Low Floating Temperature
Base Case	Power Consumption (KWH)	442.79	433.33
	Cooling Costs ($)	144.34	141.15
Optimal Passive TES Control	Power Consumption (KWH)	445.59	434.48
	Cooling Costs ($)	143.85	140.91
	Cost Savings	-0.34%	-0.17%

From Figure 26, it can be seen that, by leaving the lights in the full size zones on, the floating temperature in the morning before occupancy can be 5°F higher than leaving the lights off. With higher starting temperature in the morning, more cooling power is consumed in order to keep the zone at a comfort level. But since the building mass is very light, the impact of morning zone

floating temperature does not affect the optimal control. In both cases, the optimal control of passive TES suggests to cool the zone to 18°C for 3 hours before occupancy. In terms of cost savings, both cases save within 0.5% due to the light mass.

12 Summary

The power consumption and cooling cost savings are summarized below.

Table 5: Comparison of Simulation and Measured Results

		Rate Ratio 4:1		Rate Ratio 2:1	
		Lab	E+	Lab	E+
Base Case	Cooling Energy Use (KWH)	436.41	433.33	436.41	433.33
	Cooling Cost ($)	64.01	62.98	40.47	39.89
Passive Only	Cooling Energy Use (KWH)	437.08	434.48	436.53	434.48
	Cooling Cost ($)	63.18	62.59	39.94	39.79
	Savings	**-1.31%**	**-0.62%**	**-1.29%**	**-0.25%**
Active Only	Cooling Energy Use (KWH)	483.07	469.41	475.33	468.82
	Cooling Cost ($)	34.00	31.44	31.85	31.41
	Savings	**-46.88%**	**-50.08%**	**-21.28%**	**-21.27%**
Combined	Cooling Energy Use (KWH)	471.97	478.89	471.97	481.33
	Cooling Cost ($)	32.61	31.55	31.69	31.68
	Savings	**-49.05%**	**-49.91%**	**-21.70%**	**-20.58%**

From Table 5 it can be observed that the EnergyPlus simulation is a surprisingly accurate prediction of the experiment. Therefore, actual savings of building energy costs can be expected by applying optimal controls from simulation results. However, it can also be concluded that the Larson HVAC Laboratory has only marginal passive building thermal storage inventory and is therefore not representative of a heavy-mass commercial building.

13 Uncertainty Analysis

An uncertainty analysis is performed for the active storage (ice-based TES) charging/discharging heat transfer rate. It is a function of the measured independent parameters, i.e. ice tank inlet/out let temperature and ice tank flow rate.

$$\dot{Q} = A\rho\dot{V}C_p(T_{outlet} - T_{inlet})$$

where,

A is a conversion factor, A=6.667e-4 (ft^3/gal)(min/hr)(ton-hr/Btu),

ρ_{brine} is the density of the brine, ρ_{brine}= 65 lbm/ft^3,

C_p is the specific heat of the brine, $C_{p,brine}$=0.85 Btu/lbm/°F,

$\dot{V}$ is the volumetric flow rate of the brine, $\dot{V}$ =105 gal/min,

T_{inlet} is the ice tank inlet temperature, T_{inlet} = 25°F,

T_{outlet} is the ice tank outlet temperature, T_{outlet} = 30°F.

Measurement errors for the density and specific heat properties of the brine are neglected.

The ice tank flow rate measurement has an absolute precision of 0.3 gal/min and an absolute bias of 0.9 gal/min. The temperature measurements have absolute precisions of 0.2°F and absolute biases of 0.3°F.

Since,

$$\theta_{\dot{V}} = \frac{\partial \dot{Q}}{\partial \dot{V}} = A\rho C_p (T_{outlet} - T_{inlet})$$

$$\theta_{T_{inlet}} = \frac{\partial \dot{Q}}{\partial T_{inlet}} = -A\rho C_p \dot{V}$$

$$\theta_{T_{outlet}} = \frac{\partial \dot{Q}}{\partial T_{outlet}} = A\rho C_p \dot{V}$$

$$B_{\dot{Q}} = [(\theta_{\dot{V}} \times B_{\dot{V}})^2 + (\theta_{T_{inlet}} \times B_{T_{inlet}})^2 + (\theta_{T_{outlet}} \times B_{T_{outlet}})^2]^{1/2}$$

$$S_{\dot{Q}} = [(\theta_{\dot{V}} \times S_{\dot{V}})^2 + (\theta_{T_{inlet}} \times S_{T_{inlet}})^2 + (\theta_{T_{outlet}} \times S_{T_{outlet}})^2]^{1/2}$$

The absolute bias, relative bias, absolute precision and relative precision of heat transfer rate can now be calculated.

The uncertainty is obtained by combining the absolute precision index and the absolute bias limit, using the additive (ADD) or the root-sum-square (RSS) models for 99% and 95% of coverage respectively.

$$U_{ADD} = (B_{\dot{Q}} + st \times S_{\dot{Q}})$$

$$U_{RSS} = [B_{\dot{Q}}^2 + (st \times S_{\dot{Q}})^2]^{1/2}$$

The student factor, *st*, is used calculate the precision uncertainty and is based on the number of observations per sample, also known as the degrees of freedom. For this case, the number of observation was obtained by dividing average time interval (5 minutes) by the time-step of the readings (10 seconds). The degree of freedom is calculated by:

$$v = \left(\frac{5\,\text{min}}{10\,\text{sec}} \times 60\,\text{sec/min} \right) - 1 = 29$$

Therefore, the measured reading is 19.98 ton ±1.7 ton with 95% coverage, with a 8.3% of relative uncertainty.